THE ASTROPHYSICAL JOURNAL, 586:693–708, 2003 April 1

The concept of reionization is fundamentally false. It is based on LCDMHC cosmology, which is false, misleading and rendered obsolete by HGD cosmology.

REIONIZATION OF HYDROGEN AND HELIUM BY EARLY STARS AND QUASARS

J. STUART B. WYITHE[1,2] AND ABRAHAM LOEB[1,3,4]

Received 2002 September 3; accepted 2002 December 3

Since there are no CDM halos, there are no halo mergers.

ABSTRACT

We compute the reionization histories of hydrogen and helium caused by the ionizing radiation fields produced by stars and quasars. For the quasars we use a model based on halo-merger rates that reproduces all known properties of the quasar luminosity function at high redshifts. The less constrained properties of the ionizing radiation produced by stars are modeled with two free parameters: (i) a transition redshift, $z_{\rm tran}$, above which the stellar population is dominated by massive, zero-metallicity stars and below which it is dominated by a Scalo mass function; and (ii) the product of the escape fraction of stellar ionizing photons from their host galaxies and the star formation efficiency, $f_{\rm esc} f_*$. We constrain the allowed range of these free parameters at high redshifts on the basis of the lack of the H I Gunn-Peterson trough at $z \lesssim 6$ and the upper limit on the total intergalactic optical depth for electron scattering, $\tau_{\rm es} < 0.18$, from recent cosmic microwave background (CMB) experiments. We find that quasars ionize helium by a redshift $z \sim 4$, but cannot reionize hydrogen by themselves before $z \sim 6$. A major fraction of the allowed combinations of $f_{\rm esc} f_*$ and $z_{\rm tran}$ leads to an early peak in the ionized fraction because of the presence of metal-free stars at high redshifts. This sometimes results in two reionization epochs, namely, an early H II or He III overlap phase followed by recombination and a second overlap phase. Even if early overlap is not achieved, the peak in the visibility function for scattering of the CMB often coincides with the early ionization phase rather than with the actual reionization epoch. Consequently, $\tau_{\rm es}$ does not correspond directly to the reionization redshift. We generically find values of $\tau_{\rm es} \gtrsim 7\%$, which should be detectable by the *MAP* satellite.

Subject headings: cosmology: theory — early universe — intergalactic medium — stars: formation

From HGD cosmology, no massive stars exist, and no stars with zero metallicity.

1. INTRODUCTION

Following cosmological recombination at a redshift $z \sim 10^3$, the baryonic gas filling up the universe became predominantly neutral. Given that this gas is known to be mostly ionized today, one arrives at two of the major questions in current extragalactic astronomy: (i) *when were the cosmic hydrogen and helium reionized?* and (ii) *which sources dominated this reionization process?* The answers to both questions are likely to be different for hydrogen and helium (see the review by Barkana & Loeb 2001). Recent observations provide preliminary answers to the first question. The absorption spectra of Sloan Digital Sky Survey quasars at $z \sim 6$ indicate that the neutral fraction of hydrogen increases significantly at $z \gtrsim 6$ (Becker et al. 2001; Fan et al. 2002), and the UV spectrum of quasars implies that helium is fully ionized only at $z \lesssim 3$ (Jacobsen et al. 1994; Tytler 1995; Davidsen et al. 1996; Hogan et al. 1997; Reimers et al. 1997; Heap et al. 2000; Kriss et al. 2001; Smette et al. 2002). The latter observations also indicate, through a cross-correlation between the hydrogen and helium forest of absorption lines (Kriss et al. 2001; Smette et al. 2002), that the ionization of helium at $z \sim 3$ had significant contributions from both quasars and stars. No analogous evidence exists for hydrogen at $z \gtrsim 6$.

In this paper we make theoretical predictions for the reionization histories of hydrogen and helium. We calculate the contribution from quasars using a model that matches all the existing observational data on the quasar luminosity function at high redshifts (see Wyithe & Loeb 2002 for details). We model the less constrained stellar contribution using two free parameters, which are in turn constrained by existing observational data. Since the recombination times of both hydrogen and helium are shorter than the age of the universe in overdense regions of the intergalactic medium (IGM), it is possible that these species experienced more than one epoch of reionization. One of the goals of our detailed study is to identify the parameter values for which multiple reionization epochs are possible.

The reionization history has important implications for the temperature and polarization anisotropies of the cosmic microwave background (CMB). Anisotropies on scales smaller than the angular size of the horizon at hydrogen reionization are suppressed by a factor $\sim e^{-\tau_{\rm es}}$, where $\tau_{\rm es}$ is the line-of-sight optical depth for electron scattering (Hu & White 1997; Haiman & Loeb 1997), and secondary anisotropies are added (Hu 2000 and references therein). Reionization is the primary source of polarization anisotropies on large angular scales (Zaldarriaga & Seljak 1997; Kamionkowski et al. 1997; Hu 2000). Polarization anisotropies might be detected in the near future by *MAP* on large angular scales (Kaplinghat 2002) or by ground-based experiments on small angular scales. So far, the available data on the temperature anisotropies of the CMB provide an upper limit of $\tau_{\rm es} \lesssim 0.18$ (Wang, Tegmark, & Zaldarriaga 2002; Bond et al. 2002). We will use this upper limit to constrain the free parameters of our model.

There is no dark energy.

Throughout the paper we assume density parameters values of $\Omega_m = 0.35$ in matter, $\Omega_b = 0.052$ in baryons, $\Omega_\Lambda = 0.65$ in a cosmological constant, and a Hubble constant of $H_0 = 65$ km s^{-1} Mpc^{-1} (or equivalently $h = 0.65$). For calculations of the Press-Schechter (1974) mass function (with the modification of Sheth & Tormen 1999) we

False. The gas exists as frozen dark matter planets in clumps of a trillion termed PGCs.

[1] Harvard-Smithsonian Center for Astrophysics, 60 Garden Street, Cambridge, MA 02138; swyithe@cfa.harvard.edu.
[2] Hubble Fellow.
[3] Institute for Advanced Study, Princeton, NJ 08540; loeb@sns.ias.edu.
[4] Guggenheim Fellow; on leave from the Astronomy Department, Harvard University.

Schild (1996) was the first to observe this population and claim it as the missing mass of a galaxy, consistent with the predictions of Gibson (1996).

assume a primordial power spectrum with a power-law index $n = 1$ and the fitting formula to the exact transfer function of cold dark matter, given by Bardeen et al. (1986). Unless otherwise noted, we adopt an rms amplitude of $\sigma_8 = 0.87$ for mass density fluctuations in a sphere of radius $8\,h^{-1}$ Mpc.

There is no cold dark matter.

2. REIONIZATION IN A CLUMPY UNIVERSE

The simplest estimate of the epoch of reionization is based on the following simple considerations. Given a comoving density of ionizing photons n_γ in a homogeneous but clumpy medium of comoving density n_0 (where the size of the H II region is much larger than the scale length of clumpiness), the evolution of the volume filling factor Q_i of ionized regions is (Haiman & Loeb 1997; Madau et al. 1999; Barkana & Loeb 2001)

$$\frac{dQ_i}{dz} = \frac{1}{n_0}\frac{dn_\gamma}{dz} - \alpha_{\rm B}\frac{C}{a^3}Q_i n_e \frac{dt}{dz}\ , \qquad (1)$$

where $\alpha_{\rm B}$ is the case B recombination coefficient, $a = 1/(1+z)$ is the scale factor, n_e is the comoving electron density, and $C \equiv \langle n_0^2\rangle/\langle n_0\rangle^2$ is the clumping factor. This equation describes statistically the transition from a fully neutral universe to a fully ionized one and yields reionization redshifts for hydrogen of around 7–12. Large uncertainties arise in both the source term and the value of the clumping factor (because more rapid recombinations lead to a slower evolution of Q_i).

A more realistic description of reionization in a clumpy medium is provided by the model of Miralda-Escudé et al. (2000). In what follows, we draw primarily from their prescription and refer the reader to the original paper for a detailed discussion of its motivations and assumptions. The model assumes that reionization progresses rapidly through islands of lower density prior to the overlap of individual cosmological ionized regions. Following overlap, the remaining regions of high density are gradually ionized. It is therefore hypothesized that at any time, regions with gas below some critical overdensity $\Delta_i \equiv \rho_i/\langle\rho\rangle$ are ionized while regions of higher density are not. The assumption of homogeneity in equation (1) implies that the volume filling factor equals the mass filling factor. Therefore, within the model of Miralda-Escudé et al. (2000) we replace dQ_i/dz by $dF_M(\Delta_i)/dz$, where

$$F_M(\Delta_i) = \int_0^{\Delta_i} d\Delta P_V(\Delta)\Delta \qquad (2)$$

is the fraction of mass in regions with overdensity below Δ_i, and $P_V(\Delta)$ is the volume weighted probability distribution for Δ. The product $Q_i C$ can be rewritten

$$R(\Delta_i) \equiv Q_i C \equiv Q_i\frac{\langle\rho^2\rangle}{\langle\rho\rangle^2} = F(\Delta_i)\frac{\int_0^{\Delta_i} d\Delta P_V(\Delta)\Delta^2}{\int_0^{\Delta_i} d\Delta P_V(\Delta)}$$
$$= \int_0^{\Delta_i} d\Delta P_V(\Delta)\Delta^2\ , \qquad (3)$$

where $F(\Delta_i)$ is the fraction of the volume with $\Delta < \Delta_i$. The quantity $\alpha_{\rm B}(1+z)^3 n_e \int_0^{\Delta_i} d\Delta P_V(\Delta)\Delta^2$ is therefore the number of recombinations per atom in the IGM per second. Note that the term analogous to the clumping factor is calculated from the volume weighted distribution. The mass fraction $F_M(\Delta_i)$ (or equivalently Δ_i) therefore evolves according to the equation

$$\frac{dF_M(\Delta_i)}{dz} = \frac{1}{n_0}\frac{dn_\gamma}{dz} - \alpha_{\rm B}\frac{R(\Delta_i)}{a^3}n_e\frac{dt}{dz}\ . \qquad (4)$$

This equation assumes that all ionizing photons are absorbed shortly after being emitted, so that there is no background ionizing field and no loss of ionizing photons because of redshift. We therefore implicitly assume that the mean free path of ionizing photons is much smaller than the Hubble length. This should be valid at redshifts not too much smaller than the overlap redshift.

The integration of equation (4) requires knowledge of $P_V(\Delta)$. Miralda-Escudé et al. (2000) found that a good fit to the volume-weighted probability distribution for the density as seen in N-body simulations has the functional form

$$P_V(\Delta)d\Delta = A\exp\left[-\frac{(\Delta^{-2/3} - C_0)^2}{2(2\delta_0/3)^2}\right]\Delta^{-\beta}d\Delta\ , \qquad (5)$$

with $\delta_0 = 7.61/(1+z)$ and $\beta = 2.23$, 2.35, and 2.48, and $C_0 = 0.558$, 0.599, and 0.611 at $z = 2$, 3, and 4. At $z = 6$ they assume $\beta = 2.5$, which corresponds to the distribution of densities of an isothermal sphere, and solve for A and C_0 by requiring the mass and volume to be normalized to unity. We repeat this procedure to find $P_V(\Delta)$ at higher redshifts. The proportionality of δ_0 to the scale factor is expected for the growth of structure in an $\Omega_m = 1$ universe or at high redshift otherwise, and its amplitude should depend on the amplitude of the power-spectrum. The simulations on which the distribution in Miralda-Escudé et al. (2000) was based assumed $\Omega_m = 0.4$ in matter, $\Omega_\Lambda = 0.6$ in a cosmological constant, and $\sigma_8 = 0.79$, close to the values used in this paper.

Equation (4) provides a good description of the evolution of the ionization fraction following the overlap of individual ionized bubbles, because the ionization fronts are exposed to the mean ionizing radiation field. However, prior to overlap, the prescription is inadequate, because of the large fluctuations in the intensity of the ionizing radiation. A more accurate model to describe the evolution of the ionized volume prior to overlap was suggested by Miralda-Escudé et al. (2000). In our notation the appropriate equation is

$$\frac{d[Q_i F_M(\Delta_{\rm crit})]}{dz} = \frac{1}{n^0}\frac{dn_\gamma}{dz} - \alpha_{\rm B}(1+z)^3 R(\Delta_{\rm crit})n_e Q_i\frac{dt}{dz} \qquad (6)$$

or

$$\frac{dQ_i}{dz} = \frac{1}{n^0 F_M(\Delta_{\rm crit})}\frac{dn_\gamma}{dz}$$
$$- \left[\alpha_{\rm B}(1+z)^3 R(\Delta_{\rm crit})n_e\frac{dt}{dz} + \frac{dF_M(\Delta_{\rm crit})}{dz}\right]$$
$$\times\frac{Q_i}{F_M(\Delta_{\rm crit})}\ . \qquad (7)$$

In this expression, Q_i is redefined to be the volume filling factor within which all matter at densities below $\Delta_{\rm crit}$ has been ionized. Within this formalism, the epoch of overlap is precisely defined as the time when Q_i reaches unity. However, we have only a single equation to describe the evolution of two independent quantities Q_i and F_M. The relative growth of these depends on the luminosity function and

spatial distribution of the sources. The appropriate value of $\Delta_{\rm crit}$ is set by the mean free path of the ionizing photons. More numerous sources can attain overlap for smaller values of $\Delta_{\rm crit}$. Assuming $\Delta_{\rm crit}$ to be constant with redshift, we find that results do not vary much (less than 10% in the optical depth to electron scattering) for values of $\Delta_{\rm crit}$ ranging from a few to a few tens. At high redshift, these $\Delta_{\rm crit}$ correspond to mean free paths comparable to the typical separations between galaxies or quasars. We assume $\Delta_{\rm crit} = 20$ (which lies between the values for galaxies and quasars) throughout the remainder of this paper.

3. THE REIONIZATION OF HYDROGEN AND HELIUM

Next we describe the joint evolution of the filling factors and ionized mass fractions for hydrogen and helium using generalizations of equations (4) and (7). Let $Q_{\rm H^+}$, $Q_{\rm He^+}$, and $Q_{\rm He^{++}}$ be the filling factors of ionized hydrogen, singly ionized helium, and doubly ionized helium, and $F_{\rm H^+}$, $F_{\rm He^+}$, and $F_{\rm He^{++}}$ be the mass-fractions of ionized hydrogen, singly ionized helium, and doubly ionized helium, within the volumes $Q_{\rm H^+}$, $Q_{\rm He^+}$, and $Q_{\rm He^{++}}$ respectively. For later use we also define[5] the fractions of ionized mass in the universe $Q^m_{\rm H^+}$, $Q^m_{\rm He^+}$, and $Q^m_{\rm He^{++}}$.

We assign the comoving densities of hydrogen and helium, $n^0_{\rm H} = 1.88 \times 10^{-7}(\Omega_b h^2/0.022)$ cm^{-3} and $n^0_{\rm He} = 0.19 \times 10^{-7}(\Omega_b h^2/0.022)$ cm^{-3}, respectively, and adopt the case B recombination coefficients[6] for H$^+$, He$^+$, and He^{++} at a temperature of 10^4 K (Osterbrock 1974; Barkana & Loeb 2001); $\alpha^{\rm H^+}_{\rm B} = 2.6 \times 10^{-13}$ cm^3 s^{-1}, $\alpha^{\rm He^+}_{\rm B} = 2.73 \times 10^{-13}$ cm^3 s^{-1}, and $\alpha^{\rm He^{++}}_{\rm B} = 13 \times 10^{-13}$ cm^3 s^{-1}. The ionizing radiation field is described by the comoving densities of ionizing photons for ionized hydrogen, singly ionized helium, and doubly ionized helium, namely, $n^{\rm H^+}_\gamma$, $n^{\rm He^+}_\gamma$, and $n^{\rm He^{++}}_\gamma$, respectively. These quantities are computed through integration of the corresponding spectra in the frequency intervals $3.29 \times 10^{15} < \nu < 5.94 \times 10^{15}$ Hz for H I, $5.94 \times 10^{15} < \nu < 1.31 \times 10^{16}$ Hz for He I (He$^+$), and $\nu > 1.31 \times 10^{16}$ Hz for He II (He^{++}). Two classes of sources, quasars and stars, contribute to the ionizing radiation field. We discuss these in turn in the following subsections.

3.1. *Ionizing Photons from Quasars*

To calculate the comoving density of ionizing photons emitted by quasars, n_γ, we integrate over both the quasar luminosity function and the mean quasar spectrum (specified in Schirber & Bullock 2002). Given the B-band quasar luminosity function $\Phi(L_B, z)$ at redshift z in units of Mpc^{-3} L_B^{-1}, we find for example

$$\frac{dn^{\rm H^+}_\gamma}{dz} = -\frac{dt}{dz}\int_0^\infty dL_B \Phi(L_B, z) \int_{3.29\times10^{15}\,{\rm Hz}}^{5.94\times10^{15}\,{\rm Hz}} d\nu \frac{L_\nu(L_B)}{h_{\rm p}\nu} \ , \quad (8)$$

where $h_{\rm p}$ is the Planck constant and $L_\nu(L_B)$ is the luminosity in units of ergs s^{-1} Hz^{-1} of a quasar with a B-band luminosity L_B. At redshifts below $z = 2.5$ we use the luminosity function of Boyle et al. (2000). At $z > 2.5$ we use the theoretical luminosity function of Wyithe & Loeb (2002); the reader is referred to the original paper for more details. This quasar evolution model successfully describes all known properties of the high-redshift quasar luminosity function (Fan et al. 2001a, 2001b) and reproduces measurements of the black hole/dark matter halo mass relation (Ferrarese 2002) as well as estimates of the quasar duty cycle (Steidel et al. 2002). Since quasars at high redshift appear similar to typical examples at low redshift (Fan et al. 2001b), the luminosity function fully determines the ionizing radiation field. We therefore have almost no freedom in our calculation of the ionizing radiation field from quasars at high redshifts. This allows us to explore the effect of different stellar radiation fields on the reionization history of the universe.

3.2. *Ionizing Photons from Stars*

To compute the comoving densities of stellar ionizing photons, n_γ, we integrate over model spectra for stellar populations in the frequency ranges quoted above to find (for each species) the total number of ionizing photons, N_γ, emitted per baryon incorporated into stars. We find

$$\frac{dn^{\rm H^+}_\gamma}{dz} = N_\gamma f_{\rm esc} f_* \frac{dF_b}{dz} n_b \ , \quad (9)$$

where n_b is the local number density of baryons, $f_{\rm esc}$ is the escape fraction for the ionizing radiation, f_* is the fraction of baryons within a galaxy that are incorporated in stars, and $F_b(z)$ is the fraction of baryons in the universe at redshift z that collapsed and cooled inside galaxies. To compute $F_b(z)$ we require the dark matter collapse fraction in halos $F_{\rm col}(z, T_{\rm min})$ with virial temperatures larger than $T_{\rm min}$, given by

$$F_{\rm col}(z, T_{\rm min}) = \frac{1}{\rho_m}\int_{M_{\rm min}(T_{\rm min})}^\infty dM M \frac{dn_{\rm ps}}{dM} \ , \quad (10)$$

where ρ_m is the comoving mass density in the universe and $dn_{\rm ps}/dM$ is the Press-Schechter (1974) mass function for dark matter halos. In regions of the universe that are neutral, the critical virial temperature (the temperature at which atomic cooling becomes efficient) is $T_{\rm min} = 10^4$ K (a circular velocity of $v_{\rm cir} \sim 10$ km s^{-1}). In reionized regions, infall of gas is suppressed below a virial temperature of $T_{\rm min} \sim 2.5 \times 10^5$ K ($v_{\rm cir} \sim 50$ km s^{-1}; Thoul & Weinberg 1996). Given $F_{\rm col}(z,\ 10^4\ {\rm K})$ and $F_{\rm col}(z,\ 2.5 \times 10^5\ {\rm K})$ we can take the baryonic collapse fraction

$$F_b(z) = Q^m_{\rm H^+} F_{\rm col}(z,\ 2.5 \times 10^5\ {\rm K}) + (1 - Q^m_{\rm H^+}) F_{\rm col}(z,\ 10^4\ {\rm K}) \ . \quad (11)$$

This prescription for calculating the stellar ionizing field will be referred to hereafter as case A. Note that $f_{\rm esc}$ could be different for hydrogen and helium; however, we adopt a single value for it assuming that this value is dictated by the geometry of the optically thick gas that allows limited escape routes which are common for all ionizing photons (Wood & Loeb 2000 and references therein).

We also consider a second evolution for the stellar ionizing field, denoted hereafter as case B. A recent study (Kauffmann et al. 2003) has shown that in a large sample of local

[5] Note that Q^m is the mass filling factor. The mass filling factors for H$^+$ and He^{++} equal $Q_{\rm H^+}F_{\rm H^+}$ and $Q_{\rm He^{++}}F_{\rm He^{++}}$, respectively. Prior to the overlap of He III regions, $Q^m_{\rm He^+} = Q_{\rm He^+}F_{\rm He^+}$. However following the overlap of He III regions, $Q^m_{\rm He^+} = F_{\rm He^+}$.

[6] At high redshift, the absorption mean free path divided by the speed of light is much smaller than the Hubble time. The appropriate recombination coefficient is therefore case B.

galaxies, the ratio $\epsilon = M_*/M_{\rm halo}$ (where M_* and $M_{\rm halo}$ are the total stellar and dark matter halo masses, respectively) scales as $\epsilon \propto M_{\rm halo}^{2/3}$ for $M_* < 3 \times 10^{10}\ M_\odot$ but is constant for larger stellar masses. Note that the star formation efficiency is proportional to ϵ. Since star formation is thought to be regulated by supernova feedback (Dekel & Silk 1986), the important quantity is the depth of the galactic potential well or, equivalently, the halo circular velocity. Using the stellar-mass Tully-Fisher relation of Bell & de Jong (2001), we find the threshold circular velocity $v_* = 176$ km s^{-1} that at $z = 0$ corresponds to a stellar mass of $3 \times 10^{10} M_\odot$. In this case we define f_* as the star formation efficiency in galaxies with circular velocities larger than v_* and calculate the effective product of the dark matter collapse fraction and star formation efficiency

$$f_* F_{\rm col}(z) = \frac{1}{\rho_m} \int_{M_{\rm min}(T_{\rm min})}^{\infty} dM \epsilon f_* M \frac{dn_{\rm ps}}{dM} \ , \qquad (12)$$

where $\epsilon = 1$ for $M > M^*_{\rm halo}$ and $\epsilon = \left(M/M^*_{\rm halo}\right)^{2/3}$ for $M < M^*_{\rm halo}$. The value of $M^*_{\rm halo}(z)$ is calculated from

$$M^*_{\rm halo}(z) = 4.3 \times 10^{10} h^{-1} \left(\frac{v_*}{176\ {\rm km\ s^{-1}}}\right)^3 \times \left(\frac{\Omega_m}{\Omega_m^z} \frac{\Delta_{\rm crit}}{18\pi^2}\right)^{-1/2} \left(\frac{1+z}{10}\right)^{-3/2} M_\odot \ , \qquad (13)$$

where $\Delta_{\rm crit} = 18\pi^2 + 82d - 39d^2$, $d = \Omega_m^z - 1$, and $\Omega_m^z = \Omega_m (1+z)^3/[\Omega_m (1+z)^3 + \Omega_\Lambda]$. Finally, the value of $f_* F_b$ required for calculation of dn_γ/dz may then be computed in analogy with case A and substituted into equation (9).

In both cases A and B we make the distinction between the ionizing radiation field caused by a possible early population of zero-metallicity stars and the metal-enriched stars observed at lower redshifts. It is thought that the primordial initial mass function favored massive stars (Bromm, Copi, & Larson 1999, 2001; Abel, Bryan, & Norman 2000; Mackey, Bromm, & Hernquist 2002). The possible existence of this population is very important for reionization because the spectrum of these stars would result in an order-of-magnitude more ionizing photons per baryon incorporated into stars (Bromm, Kudritzki, & Loeb 2001). The formation of the very massive stars was suppressed as the material out of which stars form was enriched with metals. The fraction of the ionizing photons produced by metal-free stars depends on several unknown parameters, including the mixing efficiency of metals, the environments in which new stars form, and most importantly, the threshold metallicity above which star formation is transformed from being dominated by massive stars to a Scalo (1998) initial mass function (IMF). The threshold metallicity is believed to be small; Bromm et al. (2001) argue for a threshold $Z_{\rm thresh}/Z_\odot \lesssim 10^{-3}$ of the solar metallicity value. The efficiency of mixing of metal-enriched outflows from star-forming galaxies to the surrounding IGM is even more uncertain; Scannapieco, Ferrara, & Madau (2002) find that the mass-weighted mean metallicity can reach values greater than 10^{-3} times the solar value at redshifts as high as 20, and they note that the average metallicity scales with star formation efficiency, supernovae rate, and the fraction of supernovae energy that is channeled into outflows. The average metallicity increases roughly exponentially with redshift as it is modulated by the exponential growth in the collapse fraction of baryons at high redshifts.

Since the first metals were produced by supernovae, it is reasonable to suppose that the enrichment of the IGM with metals at redshift z is proportional to the mass of baryons that has formed stars by that redshift. The average metallicity at a redshift z can then be written as

$$\frac{Z(z)}{Z_\odot} = C_{\rm metal} \frac{Z_{\rm thresh}}{Z_\odot} \int_\infty^z dz \frac{dF_b}{dz} \ , \qquad (14)$$

where $C_{\rm metal}$ is a constant. Note that the baryonic collapse fraction F_b, which is computed from equation (11), is affected by the reionization history. The formation of metal-rich stars is assumed to be proportional to the average metallicity, with the fraction reaching unity when the average metalicity of the IGM reaches $Z_{\rm thresh}/Z_\odot$. Before $Z/Z_\odot(z)$ reaches $Z_{\rm thresh}/Z_\odot$, we may approximate the fraction of star formation at redshift z that is in zero-metallicity stars to be $\{[1 - Z/Z_\odot(z)]/(Z_{\rm thresh}/Z_\odot)\}$, while after $Z/Z_\odot(z)$ reaches $Z_{\rm thresh}/Z_\odot$ we may assume all star formation to have a Scalo (1998) IMF.[7]

For a given star formation efficiency and escape fraction, the above prescription yields a characteristic redshift for the build-up of the threshold metal enrichment. The exponential growth in the collapse fraction with redshift implies that the evolution in the mode of star formation resembles a step function. We therefore define a transition redshift $z_{\rm tran}$ below which metal-rich stars with a Scalo (1998) IMF dominate the production rate of ionizing photons.

Through most of the paper we present results in terms of $z_{\rm tran}$ but return to a justification of this choice in § 7. At redshifts above $z_{\rm tran}$, we use values of N_γ calculated for each of the three species H^+, He^+, and He^{++} assuming massive ($\gtrsim 100\ M_\odot$) zero-metallicity stars and the generic spectrum calculated by Bromm, Kudritzki, & Loeb (2001). The resulting values of N_γ are ~14,020 for H^+, ~25,200 for He^+, and ~4480 for He^{++}. At lower redshifts we assume metal enriched stars (1/20th solar metallicity) with a Scalo (1998) mass function and use spectral information from the stellar population model of Leitherer et al. (1999).[8] This results in values of $N_\gamma \sim 3250$ for H^+, $N_\gamma \sim 1020$ for He^+, and $N_\gamma \sim 0.2$ for He^{++}.

3.3. *Constraints on the Evolution of* H^+, He^+, *and* He^{++} *Ionization Fronts*

The typical distance that an ionizing photon of neutral helium can travel through neutral hydrogen having a cross section $\sigma_{\rm H}(\nu)$ before the optical depth reaches unity is the absorption mean free path λ, where

$$\lambda^{-1} = \frac{\int_{5.94\times10^{15}\,{\rm Hz}}^{1.31\times10^{16}\,{\rm Hz}} d\nu (L_\nu/\nu) \sigma_{\rm H}(\nu) n_{\rm H}^0 (1+z)^3}{\int_{5.94\times10^{15}\,{\rm Hz}}^{1.31\times10^{16}\,{\rm Hz}} d\nu L_\nu/\nu} \ . \qquad (15)$$

We find $\lambda \sim 4[(1+z)/10]^{-3}$ kpc. This distance is much shorter than ~1 Mpc, which is the typical size of an H II

[7] The situation in reality is more complicated since mixing of metals is incomplete and the formation sites of new stars are correlated with the enriched regions. Our discussion uses the minimum number of free parameters to describe this complicated process.

[8] Model spectra of star-forming galaxies were obtained from http://www.stsci.edu/science/starburst99/.

region around a 10^8 $M_\odot$ halo prior to reionization (Barkana & Loeb 2001). Therefore, at $z \sim 10$ the He^+ propagation front can lead the H^+ propagation front only by a small fraction of the size of the H II region, and the excess He^+ ionizing photons photoionize additional hydrogen. On the other hand, most ionizing photons for hydrogen ($\nu > 5.94 \times 10^{15}$Hz) are not absorbed by helium, and so the expansion of the H II region is not inhibited by the presence of helium. Obviously, because of the absence of singly ionized helium, the He^{++} front cannot propagate beyond the H^+ front.

Following these considerations, we impose two restrictions on the evolution of Q_{He^+} and $Q_{He^{++}}$. First, $Q_{He^{++}} \leq Q_{H^+}$. Second, $Q_{He^+} \leq Q_{H^+} - Q_{He^{++}}$. Following helium overlap, we impose the same restrictions on the evolution of the mass fraction, i.e., $F_{He^{++}} \leq F_{H^+}$ and $F_{He^+} \leq F_{H^+} - F_{He^{++}}$. The full equations governing the evolution of the filling factors and mass fractions are presented in the Appendix. The equations are split into three cases that describe three different epochs. The evolution of the filling factors prior to hydrogen overlap are described in case I. Case II describes the evolution of the filling factors and of the ionized hydrogen mass fraction following the overlap of H II regions, but prior to the overlap of He II regions. Finally, case III describes the evolution of the ionized mass fractions following the overlap of cosmological He II regions. Figure 1 provides a schematic representation of the three epochs in reionization history.

4. REIONIZATION HISTORIES

In this section we derive reionization histories for different values of z_{tran} and $f_{esc} f_*$. These histories are shown in Figures 2 (for case A star formation) and 3 (for case B star formation).

For case A we show results for combinations of $f_{esc} f_* = 0.0005$ and 0.005 and $z_{tran} = 10.0$ and 20.0. We note the following features. Large values of $f_{esc} f_*$ allow the massive zero-metallicity stars to reionize both hydrogen and helium in the universe at very early times. If the

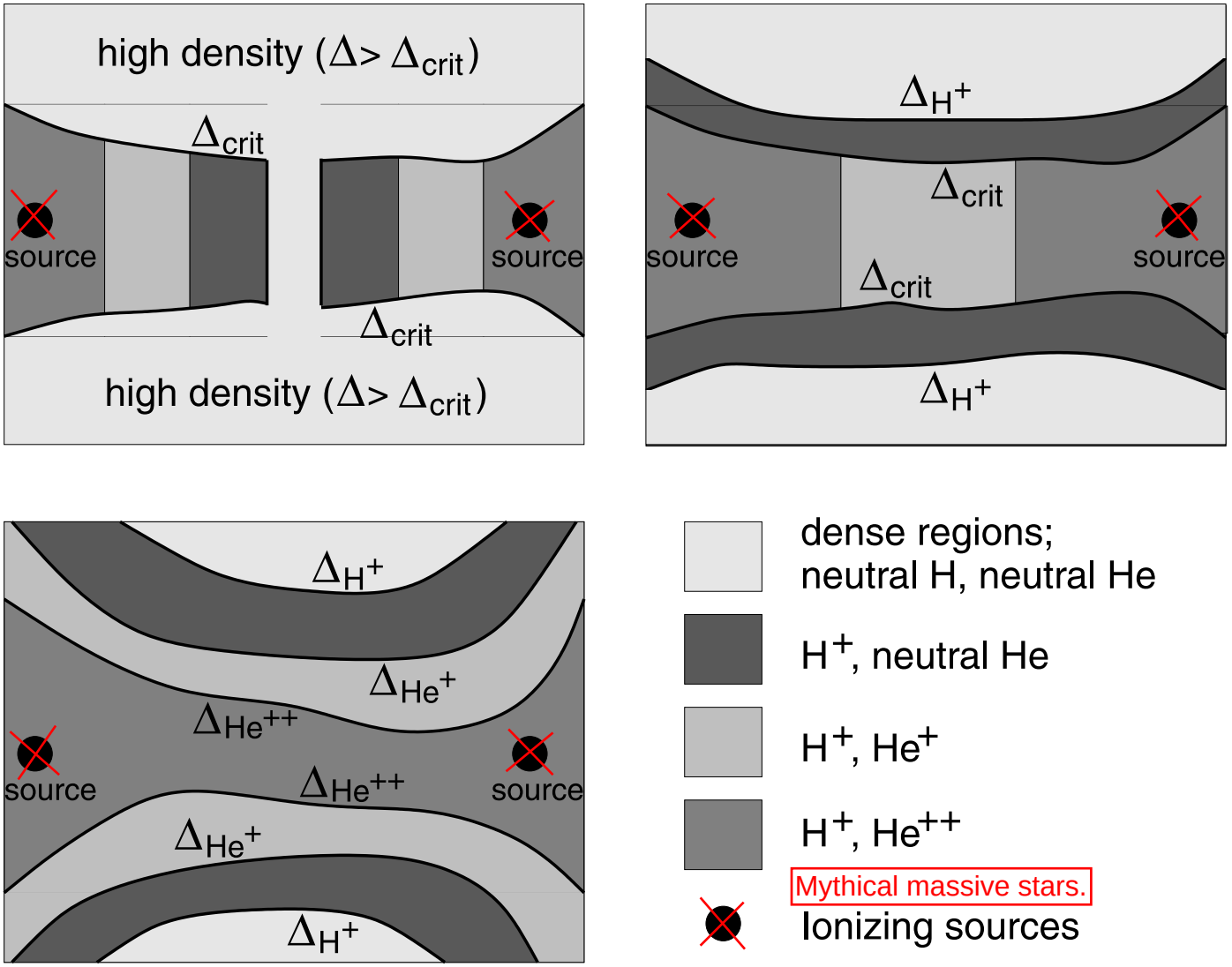

FIG. 1.—Schematic diagram of the process of reionization. Prior to the overlap of hydrogen, reionization proceeds through low-density regions (below Δ_{crit}) for both hydrogen and helium. Following the overlap of H II regions, the hydrogen reionization front moves into denser regions, but helium reionization continues to proceed through regions with density below Δ_{crit}. Finally, after the overlap of He III regions, the reionization of helium is free to proceed into denser parts of the IGM.

Stars more massive than 44% larger than the sun are unstable and explode.

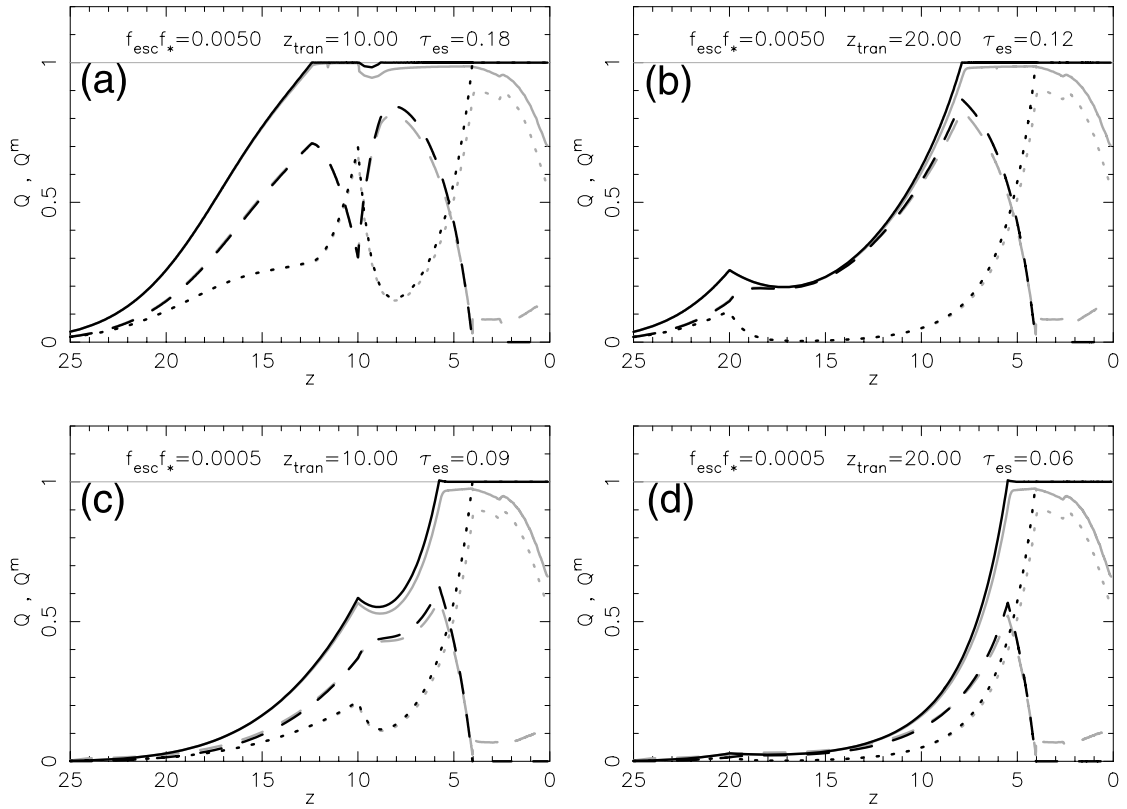

FIG. 2.—Sample reionization histories assuming case A star formation. Dark lines represent the evolution of the volume filling factors Q_{H^+}, Q_{He^+}, and $Q_{He^{++}}$, while the light lines show the evolution of the fractions of ionized mass in the universe $Q^m_{H^+}$, $Q^m_{He^+}$, and $Q^m_{He^{++}}$. The solid, dashed, and dotted lines refer to H^+, He^+, and He^{++}, respectively.

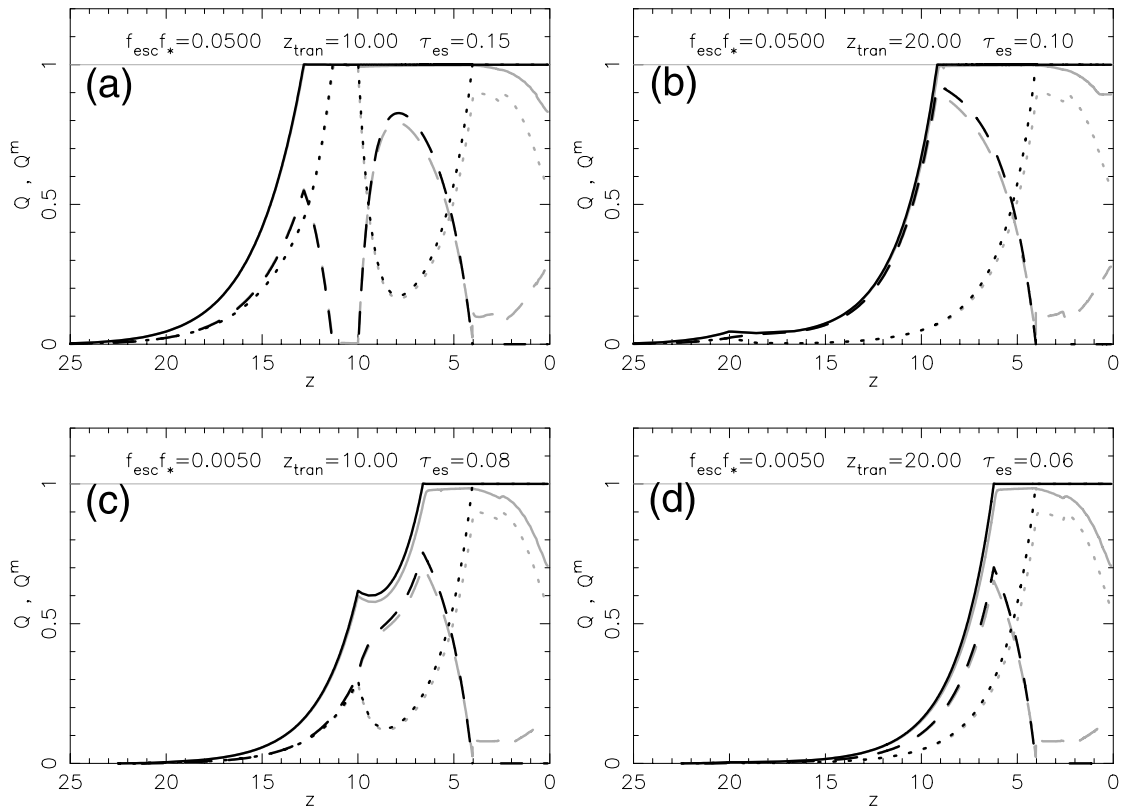

FIG. 3.—Sample reionization histories assuming case B star formation. Dark lines represent the evolution of the volume filling factors Q_{H^+}, Q_{He^+}, and $Q_{He^{++}}$, while the light lines show the evolution of the fractions of ionized mass in the universe $Q^m_{H^+}$, $Q^m_{He^+}$, and $Q^m_{He^{++}}$. The solid, dashed, and dotted lines refer to H^+, He^+, and He^{++}, respectively.

zero-metallicity stars do not reionize helium, quasars result in the overlap of He II regions by $z \sim 4$, consistent with observations that show transmission just blueward of the helium Lyα line at $z \sim 3$ (Jacobsen et al. 1994; Tytler 1995; Davidsen et al. 1996; Hogan et al. 1997; Reimers et al. 1997; Heap et al. 2000; Kriss et al. 2001; Smette et al. 2002) as well as evidence for a temperature rise in the IGM at $z \sim 3.4$ indicating the reionization of helium at that time (Schaye et al. 2000; Theuns et al. 2002). Interestingly, we also find that it is possible for hydrogen and/or helium to have been reionized twice. This situation arises if the zero-metallicity stars reionize the universe prior to $z_{\rm tran}$, but below $z_{\rm tran}$ the recombination rate is sufficiently high that the softer spectra of normal stars cannot maintain overlap. Overlap of H II regions is then reachieved at a later time as the collapse fraction grows and the density of the IGM is lowered. A second overlap of He II regions results from the rise in quasar activity at $z \lesssim 10$. Similar results are found in case B, for values of $f_{\rm esc} f_*$ that are a factor of $\sim$10 larger than in case A.

We would like to reiterate the point that multiple reionization epochs occur for some sets of parameters as a result of multiple peaks in the emissivity of ionizing photons as a function of cosmic time. In such cases the first emissivity peak occurs at $z_{\rm tran}$, at which point it drops on account of the softer spectra of metal-enriched stars. Later, when the collapsed fraction of baryons has reached a sufficiently high value, the resulting increase in emissivity further reionizes the IGM. As we will show in § 7, this double-peaked behavior is still seen if a smoothly varying fraction of collapsed objects at metallicities below the threshold produces the hard spectra rather than sources emitting prior to a fixed $z_{\rm tran}$. A double-peaked emissivity will always arise so long as the relevant metal enrichment time is less than the time required for the collapse fraction to change by a factor equal to the ratio between the emissivities of the first generation of stars and subsequent metal-enriched stars.[9]

There are two small, sharp jumps in the reionization histories that are artifacts but warrant explanation. The first is in the evolution of $Q^m_{\rm He^+}$ immediately following the overlap of He III regions. This small jump (note that the curve is smooth, not discontinuous) arises because our formalism demands $Q^m_{\rm He^+} = 0$ at this epoch. However following the overlap of $\rm He^{++}$, the $\rm He^+$ front is free to rapidly expand, powered by the strong ionizing radiation field, and the mass fraction $F_{\rm He^+}$ therefore grows until the $\rm He^+$ front reaches the $\rm H^+$ front. The second jump occurs at $z = 2.5$, where we switch from computation of the ionizing flux on account of quasars using the model quasar luminosity function to calculation using the empirical luminosity function. Neither is a perfect description around this redshift, and there is a discontinuous jump in the luminosity density, and hence in the ionizing radiation density, resulting in a jump in the reionization histories.

At early times the rise in temperature associated with reionization curtails star formation. The effect of this is clearly seen in panel *a* of Figure 2. Here the zero-metallicity stars rapidly increase the ionized fraction, but as $Q_{\rm H^+}$ approaches unity, the ionizing flux is reduced, and the rate of reionization slows. This feature is not seen in cases where overlap occurs at lower redshift (e.g., Fig. 2*d*). Many combinations of the parameters $z_{\rm tran}$ and $f_{\rm esc} f_*$ predict significant reionization without overlap due to the early presence of metal-free stars, resulting in a peak in the ionized fraction centered on the transition redshift, followed by recombinations before further reionization on account of normal stars and quasars. We term these peaks "failed overlaps." In § 6 we show that these failed overlaps leave a significant imprint on the visibility function for electron scattering of CMB photons.

[9] Note that even if the mixing of metals is partial and the intergalactic filling factor of metals is smaller than unity (e.g., Scannapieco et al. 2002), new stars are likely to form in regions that were already enriched because galaxies tend to be clustered on large-scale sheets and filaments. This effect needs to be included when evaluating the effective $z_{\rm tran}$ from numerical simulations.

4.1. *The Optical Depth to Electron Scattering*

Different reionization histories result in different densities of electrons as a function of redshift. One simple probe of the reionization history is the optical depth to electron scattering $\tau_{\rm es}$, which depend on the mass filling factors Q^m

$$\tau_{\rm es} = \int_0^{1000} dz \frac{c\,dt}{dz} \sigma_{\rm T} \left[Q^m_{\rm H^+} n^0_{\rm H} + Q^m_{\rm He^+} n^0_{\rm He} + 2 Q^m_{\rm H^{++}} n^0_{\rm He} \right] \times (1+z)^3 \,, \quad (16)$$

where $\sigma_{\rm T} = 6.652 \times 10^{-25}$ cm^2 is the Thomson cross section. In the following section we plot contours of $\tau_{\rm es}$ as a function of $z_{\rm tran}$ and $f_{\rm esc} f_*$.

5. JOINT CONSTRAINTS ON $z_{\rm tran}$ AND $f_{\rm esc} f_*$

In this section we discuss the constraints that current observations place on $z_{\rm tran}$ and $f_{\rm esc} f_*$. First we discuss the variation of $\tau_{\rm es}$ with $z_{\rm tran}$ and $f_{\rm esc} f_*$. The optical depth for electron scattering is constrained from recent CMB anisotropy experiments to a value $\tau_{\rm es} < 0.18$ (Wang & Tegmark 2002). An upper limit on $\tau_{\rm es}$ implies that there is maximum redshift beyond which the universe was neutral. As a second constraint, we note that the spectra of quasars at $z \lesssim 6$ do not show a Gunn-Peterson (1965) trough, indicating that H II regions had achieved overlap earlier than that time.

As we have seen in the previous section, the universe is reionized earlier for higher values of $f_{\rm esc} f_*$, which results in higher values of $\tau_{\rm es}$. Hence $f_{\rm esc} f_*$ cannot be too large so as not to violate the limit $\tau_{\rm es} < 0.18$. On the other hand, if the product $f_{\rm esc} f_*$ is too small, then the ionizing radiation field will be too weak for the H II regions to overlap by $z \sim 6$. If the transition redshift $z_{\rm tran}$ is large, then $f_{\rm esc} f_*$ may obtain higher values since the harder spectra of metal-free stars are available only to the ionizing radiation field at high redshifts when the IGM is dense and the collapse fraction is small. However, if $z_{\rm tran}$ is low, then $f_{\rm esc} f_*$ may take smaller values and still result in overlap of H II regions by $z \sim 6$. In addition to the above constraints, observations suggest that the IGM was metal enriched by $z \sim 6$ (Songaila 2001) to a level that would lead to a Scalo stellar mass function (Bromm et al. 2001) if new galaxies formed out of it. As a result, $z_{\rm tran}$ is limited to be larger than 6.

Figures 4 and 5 show contours of $\tau_{\rm es}$ (*solid lines*) as a function of $z_{\rm tran}$ and $f_{\rm esc} f_*$ for case A and B star formation, respectively. Also shown are contours of $Q_{\rm H^+}$ at $z = 6$ (*dashed lines*) and a vertical line at $z_{\rm tran} = 6$ (*dot-dashed line*). The regions excluded by the aforementioned constraints are shaded gray. For our case A star formation model we find

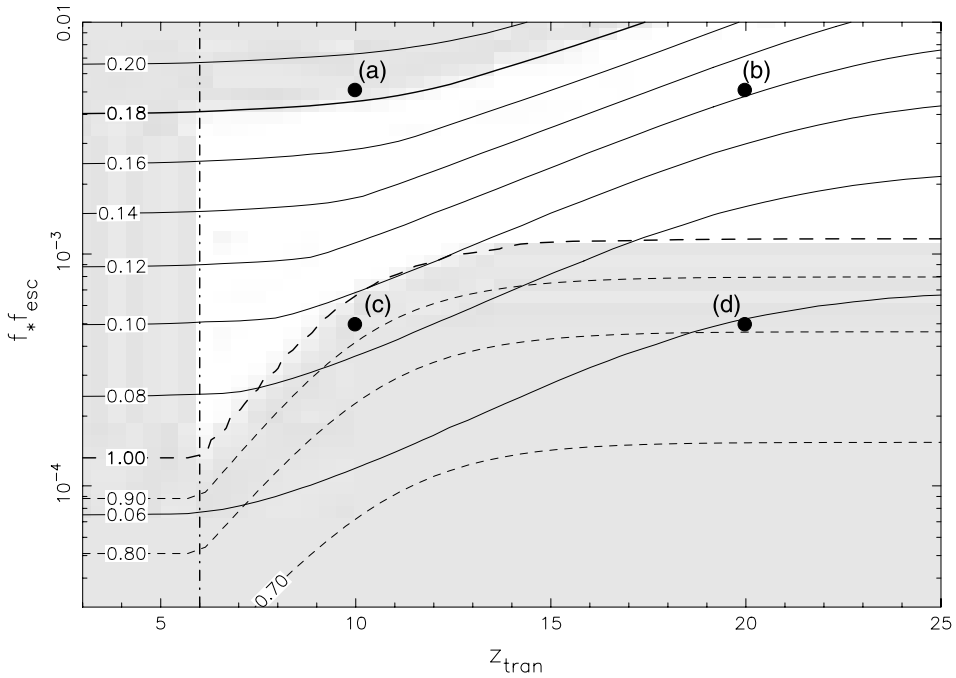

FIG. 4.—Contours of optical depth for Thomson scattering, τ_{es} (*solid lines*), and contours of Q_{H^+} at $z = 6$ (*dashed lines*), as a function of $f_{esc} f_*$ and z_{tran}. Case A star formation was assumed, and the shaded regions are excluded by existing observations. The four labeled points refer to the locations of the parameter sets used in the example histories presented in Fig. 2.

that $f_{esc} f_* \lesssim 0.004$ if $z_{tran} \lesssim 10$. For a higher z_{tran}, we find that larger values of $f_{esc} f_*$ are possible. If $z_{tran} \sim 6$, $f_{esc} f_*$ may be as low as 10^{-4}, though for $z_{tran} \geq 15$ we find $f_{esc} f_* \gtrsim 0.001$. We find that the lower limits on $f_{esc} f_*$ are larger by a factor of $\sim$3 for our case B star formation model. However, since the intensity of the stellar radiation field is curtailed by feedback at high redshift in this model, we find that $f_{esc} f_*$ can be as large as $\sim$0.1 for $z_{tran} \lesssim 15$, or even larger for $z_{tran} \gtrsim 15$. Interestingly, the contours for τ_{es} and z_{reion} are not parallel. A significant range of τ_{es} exist for different z_{tran} (particularly where case A star formation is assumed). This indicates that measurement of optical depth does not determine the overlap redshift. We discuss the reason for this puzzling result in § 6.

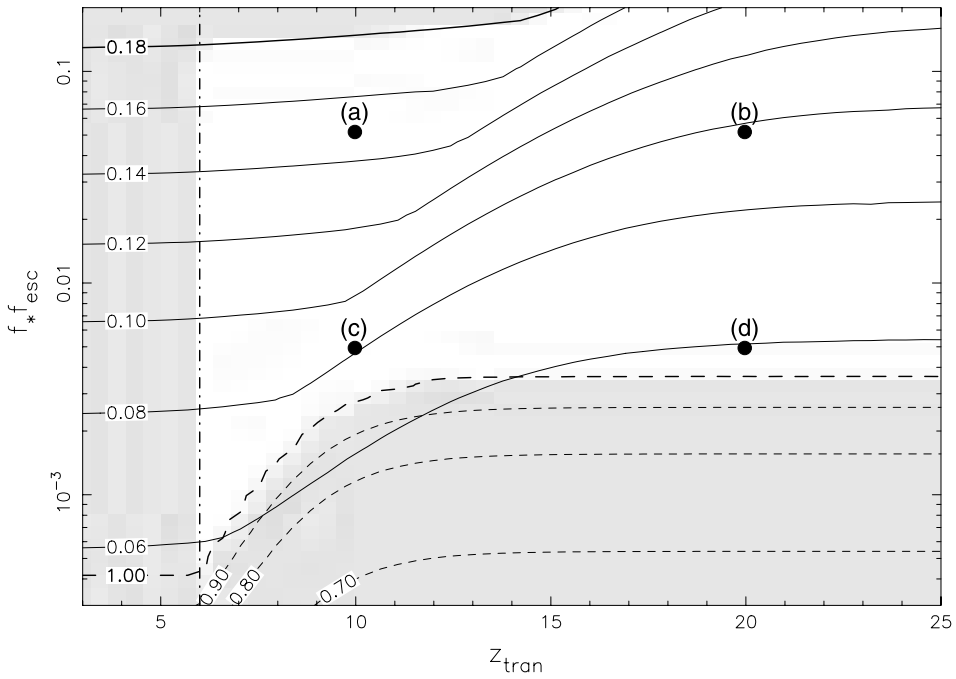

FIG. 5.—Contours of optical depth for Thomson scattering, τ_{es} (*solid lines*), and contours of Q_{H^+} at $z = 6$ (*dashed lines*), as a function of $f_{esc} f_*$ and z_{tran}. Case B star formation was assumed, and the shaded regions are excluded by existing observations. The four labeled points refer to the locations of the parameter sets used in the example histories presented in Fig. 3.

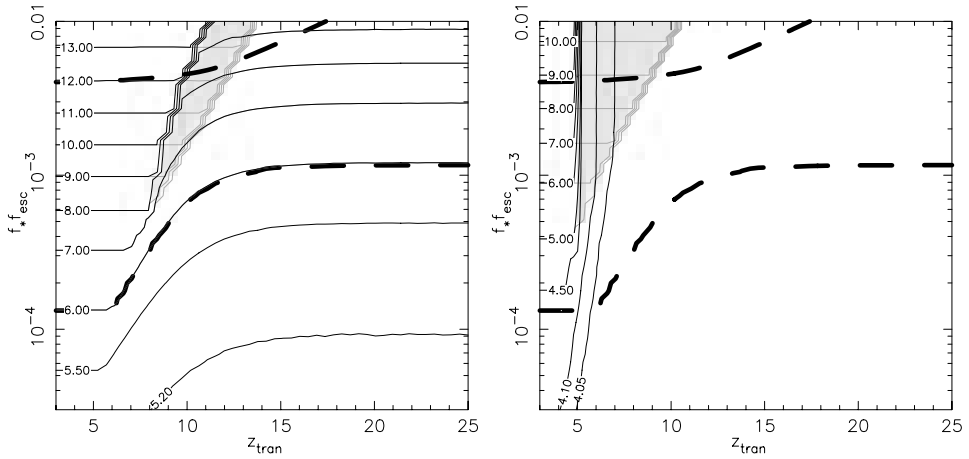

FIG. 6.—Contours of overlap redshift for hydrogen (*left panel*) and fully ionized helium (*right panel*), as a function of $f_{esc} f_*$ and z_{tran} assuming case A star formation. The dark contours show the most recent overlap. Parameter pairs that produce two overlap epochs lie in the shaded region. The gray contours describe the redshifts of these earlier overlaps. Note that the regions below and to the right of the lowest redshift contour shown have nearly constant overlap redshift. This arises because quasars dominate the reionization process for these parameter pairs. Also shown for reference are the contours of $\tau_{es} = 0.18$ and $Q_{H^+} = 1$ at $z = 6$ (*thick dashed lines*). Parameter pairs not lying between these lines are excluded by current observation.

In § 4 we mentioned that hydrogen and/or helium could be reionized twice and showed examples of reionization histories that exhibit this behavior. In Figures 6 and 7 we show contours of the overlap redshift for hydrogen (*left panels*) and helium (*right panels*), for case A and case B star formation models. The redshift of the most recent overlap is described by the dark contours. At high values of z_{tran} and low values of $f_{esc} f_*$, the overlap redshift is almost independent of star formation since then quasars dominate the ionizing radiation field. This is particularly true for helium, which is ionized by quasars at $z \sim 4$ in the absence of any stellar ionizing radiation. Cases where there was an additional earlier overlap are denoted by the gray contours. The region of the $(z_{tran}, f_{esc} f_*)$ plane that results in multiple overlap epochs is shaded gray. We see that this area covers a significant portion of parameter space, and therefore that it is quite possible the universe was reionized twice. The contours representing the upper limit of $\tau_{es} < 0.18$, and the lower limit for the overlap redshift $z > 6$ are also shown (*thick dashed lines*). As mentioned earlier, parameters in the region between these limits are not excluded by current observations.

6. THE VISIBILITY FUNCTION

The visibility function $g(z)d\eta$ describes the probability that an observed photon was scattered between conformal times $\eta(z)$ and $\eta + \Delta\eta$:

$$g(z) = \frac{d\tau_{es}}{d\eta} e^{-\tau_{es}} = \sigma_T \left[Q^m_{H^+} n^0_H + Q^m_{He^+} n^0_{He} + 2 Q^m_{He^{++}} n^0_{He} \right] \times (1+z)^2 e^{-\tau_{es}} , \quad (17)$$

where $d\eta = (1+z) c\, dt$, τ_{es} is the optical depth from redshift 0 to z and the Q^m are mass filling factors. It is commonly assumed that the visibility function is peaked during the

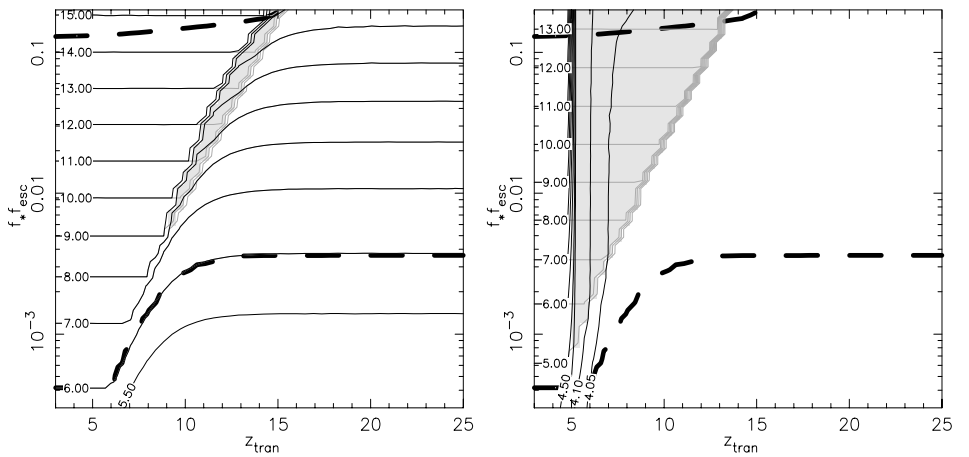

FIG. 7.—Contours of overlap redshift for hydrogen (*left panel*) and fully ionized helium (*right panel*), as a function of $f_{esc} f_*$ and z_{tran} assuming case B star formation. The dark contours show the most recent overlap. Parameter pairs that produce two overlap epochs lie in the shaded region. The gray contours describe the redshifts of these earlier overlaps. Note that the regions below and to the right of the lowest redshift contour shown have nearly constant overlap redshift. This arises because quasars dominate the reionization process for these parameter pairs. Also shown for reference are the contours of $\tau_{es} = 0.18$ and $Q_{H^+} = 1$ at $z = 6$ (*thick dashed lines*). Parameter pairs not lying between these lines are excluded by current observation.

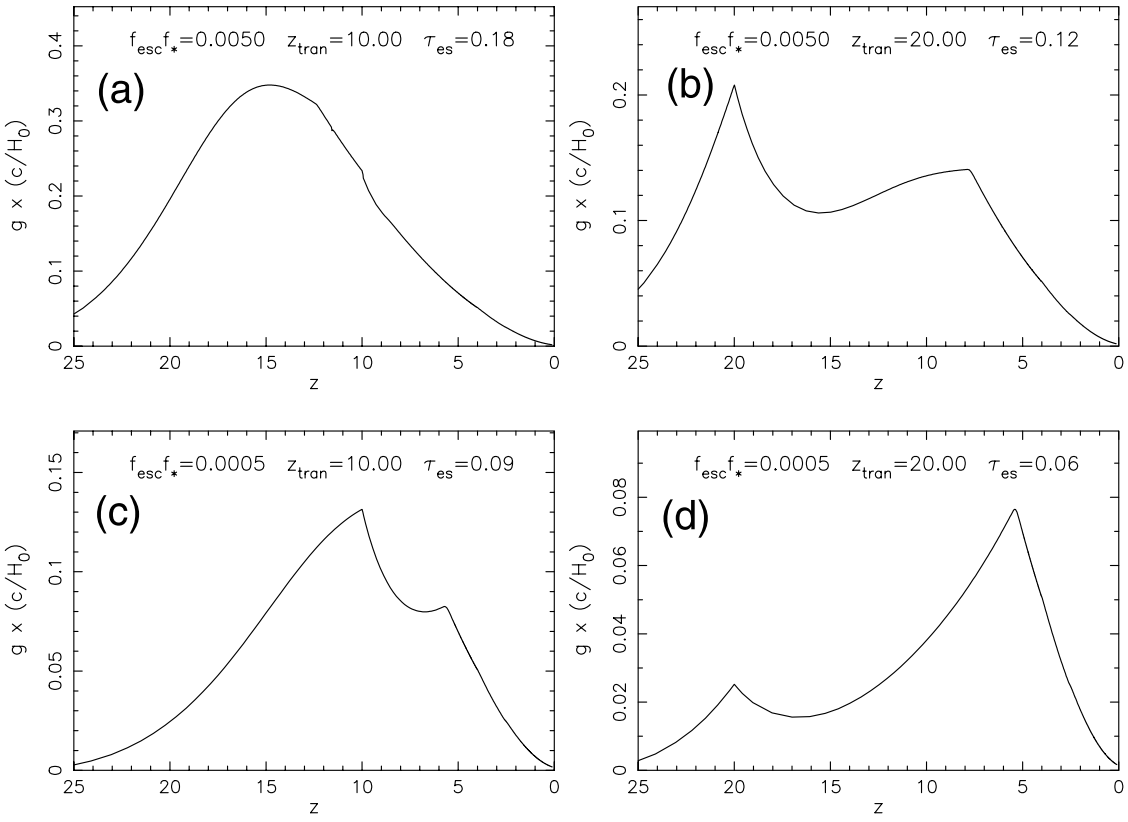

FIG. 8.—Sample visibility functions (in units of H_0/c). The four cases correspond to the sample reionization histories (assuming case A star formation) plotted in Fig. 2.

recombination era, with a second, lower amplitude, but broader peak coinciding with the epoch of overlap of H II regions. However, we have found that overlap may have occurred on multiple occasions and that many combinations of the parameters $z_{\rm tran}$ and $f_{\rm esc} f_*$ predict significant reionization without overlap (*failed overlap*) at high redshift due to the early presence of metal-free stars. During these failed overlaps, examples of which are shown in Figures 2 and 3, the ionization fraction can be significant. Following a failed overlap at $z_{\rm tran}$, recombinations dominate the evolution and the ionization fraction drops before further reionization ensues on account of normal stars and quasars. The higher cosmic density at early times might more than compensate for the smaller ionization fraction, so that the peak of the visibility function does not coincide with the epoch of reionization.

This is indeed what we find. Figures 7 and 8 show visibility functions corresponding to the sample reionization histories shown in Figures 2 and 3. Generally, if the early metal-free stars succeed in achieving reionization, then the peak in the visibility function coincides with this overlap epoch (e.g., case A in Figs. 2 and 3). However the optical depth $\tau_{\rm es}$ is large, and many of these cases are already excluded by CMB measurements. Of the eight cases shown in Figures 2 and 3, those that exhibit failed overlap have visibility peaks that coincide with this failed overlap, rather than with the actual reionization epoch. *Thus, the visibility function may probe the nature of the early generation of stars rather than the reionization epoch itself.*

The reionized gas during a failed overlap will be in bubbles. Gruzinov & Hu (1998) have pointed out that a universe which is ionized in patches induces additional CMB anisotropies on arcminute scales. Thus, patchy reionization caused by a failed overlap at high redshifts will modify the shape of the small-scale power spectrum of CMB anisotropies. However, the amplitude of the added secondary anisotropies was predicted to be at a level well below the feature in the spectrum detected more recently by the Cosmic Background Imager (Padin et al. 2001). This feature was explained by Bond et al. (2002) as being due to the foreground Sunyaev-Zeldovich effect from X-ray clusters.

7. JUSTIFICATION FOR STEP FUNCTION APPROACH TO THE EVOLUTION IN THE MODE OF STAR FORMATION

As mentioned in § 3.2 we have approximated the evolution in the mode of star formation as a step function. That is, we have assumed that the production rate of ionizing photons in the universe is transformed sharply at $z_{\rm tran}$ from being dominated by massive, metal-free stars to being dominated by metal-rich stars with a Scalo IMF. In this section we justify this approach by comparing its results to those obtained with a scheme involving gradual metal enrichment of the IGM as described in § 3.2 by equation (14).

Figure 10 shows two sample reionization histories computed using the gradual enrichment scheme, together with the resulting visibility function. The examples correspond to panels *a* and *c* for Case B star formation in Figure 3. The thick grey line in these panels shows the fraction of star formation resulting in a Scalo (1998) mass function as a function of redshift. In each of these cases the value of $C_{\rm metal}$

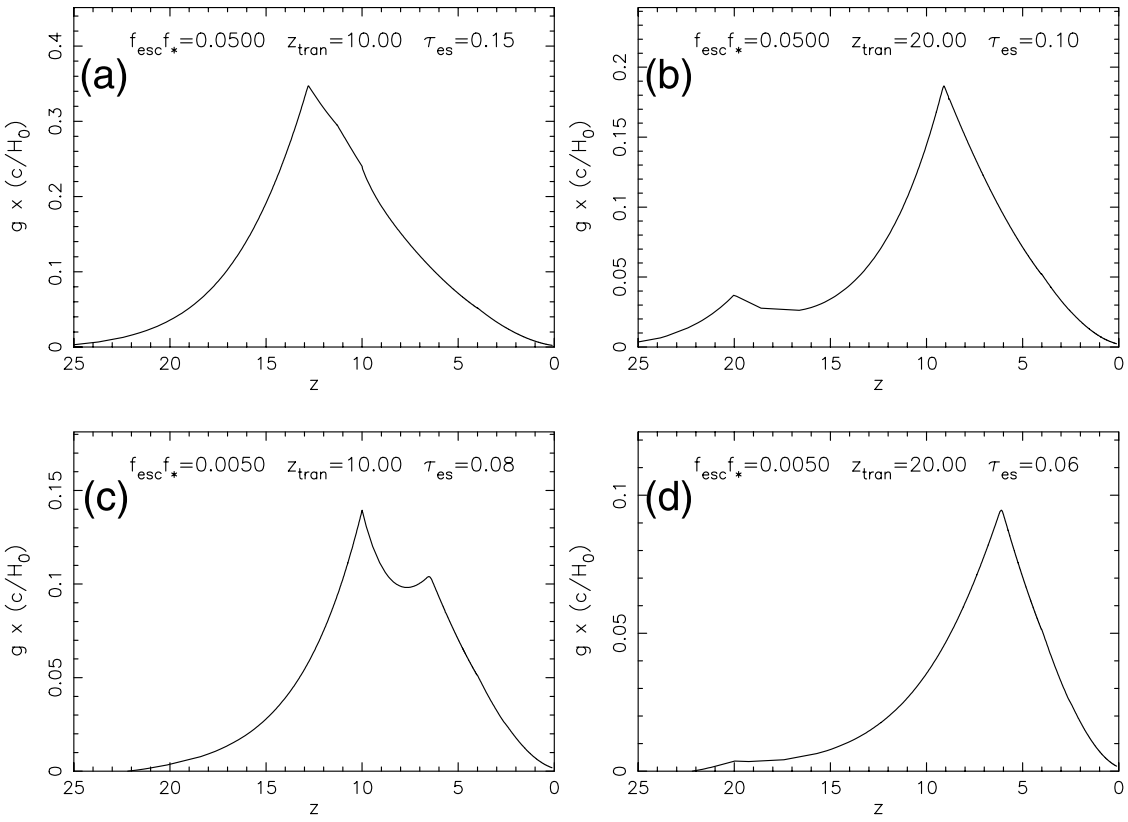

FIG. 9.—Sample visibility functions (in units of H_0/c). The four cases correspond to the sample reionization histories (assuming case B star formation) plotted in Fig. 3.

(listed in the figure) produces around 50% Scalo (1998) IMF star formation at the previously used redshift z_{tran}. Note the different values of C_{metal}, and the different histories of the collapsed mass-fraction. The features discussed for the corresponding examples in Figures 3 and 9 are still present in Figure 10. These include the double overlap of He III in *a*, and the non coincidence of the overlap redshift of H II and the peak in the visibility function in *b*. Furthermore, we find unchanged values of τ_{es}. These calculations appear to justify our use of a single parameter z_{tran} to characterize the reionization histories and visibility functions.

There never were any massive stars.

8. CONCLUSION

We have explored the reionization histories of hydrogen and helium caused by stars and quasars. The results were analyzed as a function of the two free parameters in our model, namely, (i) the transition redshift, z_{tran}, above which the stellar population is dominated by massive, zero-metallicity stars; and (ii) the product of the escape fraction of ionizing photons and the star formation efficiency, $f_{esc}f_*$. The quasar model was not varied since it provides an excellent fit to all existing data on the luminosity function of quasars up to redshift $z \sim 6$ (Wyithe & Loeb 2002).

Figures 2 and 3 show sample reionization histories for different choices of z_{tran} and $f_{esc}f_*$. We find that a wide range of $z_{tran} \gtrsim 6$ is allowed for $f_{esc}f_* \sim 2 \times 10^{-3}$ if the star formation efficiency does not depend on galaxy mass (Fig. 4) or $f_{esc}f_* \sim 10^{-2}$ if the efficiency is suppressed in low-mass galaxies (Fig. 5). This wide range satisfies the constraints that overlap of the H II regions must be achieved by $z \sim 6$ (Fan et al. 2002) and that the optical depth for electron scattering must be limited to $\tau_{es} < 0.18$. The allowed range leads generically to $\tau_{es} \gtrsim 7\%$ (see Figs. 4 and 5). The *MAP* satellite is expected to have sufficient sensitivity to detect values of τ_{es} as small as $\sim 5\%$ (Kaplinghat et al. 2002), well below this range of expected values.

A major fraction of the allowed range of $f_{esc}f_*$ and z_{tran} leads to an early peak in the ionized fraction because of the presence of metal-free stars at high redshifts. Often this peak results in a small but significant filling factor that is subsequently reduced (temporarily) because of recombination. In a restricted range of the allowed parameter values, we find that either hydrogen or helium experience two overlap epochs, separated by recombination (see shaded regions in Figs. 6 and 8). That helium might have been reionized twice because of the presence of early very massive stars was previously pointed out by Oh et al. (2001). The first overlap phase is caused by the population of zero-metallicity, massive stars, and the second is dominated by the quasars for helium or by stars and quasars for hydrogen. Even if early overlap is not achieved, the peak in the visibility function for scattering of the CMB often coincides with the early partial ionization peak rather than with the actual reionization epoch (see Figs. 7 and 9). The resulting value of τ_{es} is therefore larger than expected based the reionization redshift alone. Thus, the CMB visibility function may be probing the nature of the early generation of stars rather than the reionization epoch itself.

Future CMB experiments, such as *MAP* and *Planck*, will provide tighter constraints on τ_{es} and will reduce the range of allowed $f_{esc}f_*$ in our model (see Figs. 4 and 5). Any

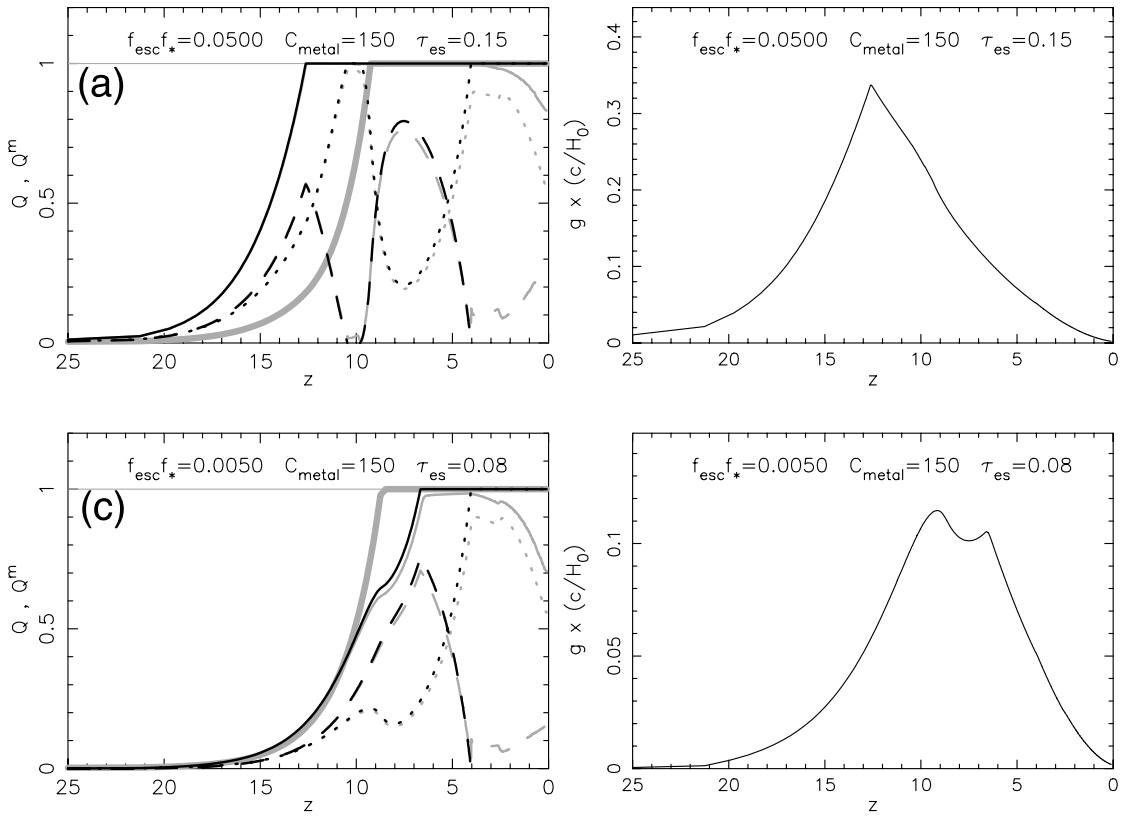

FIG. 10.—Results for reionization histories computed assuming continuous enrichment of the IGM rather than sudden enrichment at $z_{\rm tran}$. The results should be compared with panels *a* and *c* of Figs. 3 and 9. *Left*: Sample reionization histories assuming case B star formation. Dark lines represent the evolution of the volume filling factors $Q_{\rm H^+}$, $Q_{\rm He^+}$, and $Q_{\rm He^{++}}$, while the light lines show the evolution of the fractions of ionized mass in the universe $Q^m_{\rm H^+}$, $Q^m_{\rm He^+}$, and $Q^m_{\rm He^{++}}$. The solid, dashed, and dotted lines refer to H^+, He^+, and He^{++}, respectively. *Right*: The corresponding visibility functions (in units of H_0/c).

additional observational data on the composition of the stellar population or the abundance of He I or He II at $z \gtrsim 4$ will provide stronger lower limits on $z_{\rm tran}$.

We thank Rennan Barkana and an anonymous referee for useful detailed comments on the manuscript. J. S. B. W. is supported by a Hubble Fellowship grant from the Space Telescope Science Institute, which is operated by the Association of Universities for Research in Astronomy, Inc., under NASA contract NAS 5-26555. A. L. acknowledges generous support from the Institute for Advanced Study at Princeton University and the John Simon Guggenheim Memorial Fellowship. This work was also supported in part by NSF grant AST 00-71019.

The paper is based on the false premise that cold dark matter exists. It does not. CDM was invented because the Jean's scale of the plasma epoch was always larger than the scale of causal connection ct, where c is the speed of light and t is the time since the cosmological big bang. The Jeans scale is the speed of sound times the gravitational free fall time. It was hoped that by reducing the temperature of the unknown massive nonbaryonic component of the universe that somehow this would reduce its speed of sound and permit condensation of small CDM seeds that could clump together to form more massive CDM halos that would gravitationally trap the baryons needed to make stars. This is LCDMHC cosmology, and it is hopelessly wrong in its fluid mechanics as shown by Gibson (1996), and abundantly falsified by all available observations, starting with the gravitational microlensing of a quasar by a galaxy as described by Schild (1996).

APPENDIX A

EQUATIONS DESCRIBING REIONIZATION OF HYDROGEN AND HELIUM IN A CLUMPY UNIVERSE

The filling factors Q_{H^+}, Q_{He^+}, and $Q_{He^{++}}$, and ionized mass fractions F_{H^+}, F_{He^+}, and $F_{He^{++}}$ evolve according to six coupled ordinary differential equations (ODEs). It is convenient to write the ODEs and constraints in terms of the following quantities:

$$
\begin{aligned}
S_{\rm CF}^{\rm H^+} &= \frac{1}{n_{\rm H}^0}\frac{dn_\gamma^{\rm H^+}}{dz}\ ,\\
S_{\rm CF}^{\rm He^+} &= \frac{1}{n_{\rm He}^0}\frac{dn_\gamma^{\rm He^+}}{dz}\ ,\\
S_{\rm CF}^{\rm He^{++}} &= \frac{1}{n_{\rm He}^0}\frac{dn_\gamma^{\rm He^{++}}}{dz}\ ,\\
S_{\rm C}^{\rm H^+} &= \frac{1}{n_{\rm H}^0 F_{\rm H^+}}\frac{dn_\gamma^{\rm H^+}}{dz}\ ,\\
S_{\rm C}^{\rm He^+} &= \frac{1}{n_{\rm He}^0 F_{\rm He^+}}\frac{dn_\gamma^{\rm He^+}}{dz}\ ,\\
S_{\rm C}^{\rm He^{++}} &= \frac{1}{n_{\rm He}^0 F_{\rm He^{++}}}\frac{dn_\gamma^{\rm He^{++}}}{dz}\\
S_{\rm KF}^{\rm H^+} &= \alpha_{\rm B}^{\rm H^+}\frac{R^{\rm H^+}}{a^3}n_e^{\rm H^+}\frac{dt}{dz}\ ,\\
S_{\rm KF}^{\rm He^+} &= \alpha_{\rm B}^{\rm He^+}\frac{R^{\rm He^+}}{a^3}n_e^{\rm He^+}\frac{dt}{dz}\ ,\\
S_{\rm KF}^{\rm He^{++}} &= \alpha_{\rm B}^{\rm He^{++}}\frac{R^{\rm He^{++}}}{a^3}n_e^{\rm He^{++}}\frac{dt}{dz}\ ,\\
S_{\rm K}^{\rm H^+} &= \left(\alpha_{\rm B}^{\rm H^+}\frac{R^{\rm H^+}}{a^3}n_e^{\rm H^+}\frac{dt}{dz}+\frac{dF_{\rm H^+}}{dz}\right)\frac{Q_{\rm H^+}}{F_{\rm H^+}}\ ,\\
S_{\rm K}^{\rm He^+} &= \left(\alpha_{\rm B}^{\rm He^+}\frac{R^{\rm He^+}}{a^3}n_e^{\rm He^+}\frac{dt}{dz}+\frac{dF_{\rm He^+}}{dz}\right)\frac{Q_{\rm He^+}}{F_{\rm He^+}}\ ,\\
S_{\rm K}^{\rm He^{++}} &= \left(\alpha_{\rm B}^{\rm He^{++}}\frac{R^{\rm He^{++}}}{a^3}n_e^{\rm He^{++}}\frac{dt}{dz}+\frac{dF_{\rm He^{++}}}{dz}\right)\frac{Q_{\rm He^{++}}}{F_{\rm He^{++}}}\ .
\end{aligned}
\tag{A1}
$$

In the above definitions, the $S_{\rm C}$ and $S_{\rm CF}$ are source terms describing the ionizing radiation field, while the $S_{\rm K}$ and $S_{\rm KF}$ are sink terms describing the recombination rate. In the recombination terms, the n_e are the electron densities available for recombination (equal to the mean cosmological density multiplied by the volume filling factor and the mass fraction). These are therefore

$$
\begin{aligned}
n_e^{\rm H^+} &= \left(n_{\rm H}^0 + n_{\rm He}^0\frac{Q_{\rm He^+}F_{\rm He^+}+2Q_{\rm He^{++}}F_{\rm He^{++}}}{Q_{\rm H^+}F_{\rm H^+}}\right)\ ,\\
n_e^{\rm He^+} &= \left(n_{\rm H}^0 + n_{\rm He}^0\right)\ ,\\
n_e^{\rm He^{++}} &= \left(n_{\rm H}^0 + 2n_{\rm He}^0\right)\ .
\end{aligned}
\tag{A2}
$$

We write the generalization of equations (4) and (7) for the three species in terms of the above quantities. There are three cases corresponding to the period before H II regions overlap, the period following the overlap of H II regions but preceding the overlap of He II regions, and the period following the overlap of He II regions.

A1. CASE I: PRE HYDROGEN OVERLAP: IF $Q_{H^+} < 1$ OR $F_{H^+} < F_M(\Delta_{\rm crit})$

Prior to the overlap of H II regions, the mass fractions F and their derivatives are set by the critical value of $\Delta_{\rm crit}$ chosen as the ionization density threshold. The filling factors Q_{H^+}, Q_{He^+}, and $Q_{He^{++}}$ evolve according to a generalization of equation (4).

Hence

$$\frac{dF_{\rm H^+}}{dz} = \frac{d}{dz}F_M(\Delta_{\rm crit})F_{\rm H^+} = F_M(\Delta_{\rm crit}) ,$$
$$\frac{dF_{\rm He^+}}{dz} = \frac{d}{dz}F_M(\Delta_{\rm crit})F_{\rm He^+} = F_M(\Delta_{\rm crit}) ,$$
$$\frac{dF_{\rm He^{++}}}{dz} = \frac{d}{dz}F_M(\Delta_{\rm crit})F_{\rm He^{++}} = F_M(\Delta_{\rm crit}) ,$$
$$\frac{dQ_{\rm H^+}}{dz} = S_{\rm C}^{\rm H^+} + \frac{1}{n_{\rm H}^0 F_{\rm H^+}}\left(\Delta\frac{dn_\gamma^{\rm He^+}}{dz} + \Delta\frac{dn_\gamma^{\rm He^{++}}}{dz}\right) - S_{\rm K}^{\rm H^+} ,$$
$$\frac{dQ_{\rm He^+}}{dz} = S_{\rm C}^{\rm He^+} - \frac{1}{n_{\rm He}^0 F_{\rm He^+}}\Delta\frac{dn_\gamma^{\rm He^+}}{dz} - S_{\rm K}^{\rm He^+} - \frac{dQ_{\rm He^{++}}}{dz} ,$$
$$\frac{dQ_{\rm He^{++}}}{dz} = S_{\rm C}^{\rm He^{++}} - \frac{1}{n_{\rm He}^0 F_{\rm He^{++}}}\Delta\frac{dn_\gamma^{\rm He^{++}}}{dz} - S_{\rm K}^{\rm He^{++}} . \quad \text{(A3)}$$

In the above, $\Delta\left(dn_\gamma^{\rm He^+}/dz\right)$ and $\Delta\left(dn_\gamma^{\rm H^{++}}/dz\right)$ are the excess ionizing photon rates having frequencies $5.94\times10^{15} < \nu < 1.31\times10^{16}$ Hz for He I ionization and $\nu > 1.31\times10^{16}$Hz for He II ionization. The values of these excess source terms are determined from the constraints on the relative evolution of the different ionization fronts. As these are excess rates, their values must be positive.

If $Q_{\rm He^{++}} < Q_{\rm H^+}$, then $Q_{\rm He^+}$ is limited to be smaller than $Q_{\rm H^+} - Q_{\rm He^{++}}$ since the $\rm He^+$ front cannot propagate beyond the $\rm H^+$ front. Therefore, if $Q_{\rm He^+} = Q_{\rm H^+} - Q_{\rm He^{++}}$, we require $dQ_{\rm He^+}/dz = dQ_{\rm H^+}/dz - dQ_{\rm He^{++}}/dz$, and since $\Delta\left(dn_\gamma^{\rm He^{++}}/dz\right) = 0$ in this case, we find

$$\Delta\frac{dn_\gamma^{\rm He^+}}{dz} = \left(\frac{1}{n_{\rm He}^0 F_{\rm He^+}} + \frac{1}{n_{\rm H}^0 F_{\rm H^+}}\right)^{-1}\left[(S_{\rm C}^{\rm He^+} - S_{\rm C}^{\rm H^+}) - (S_{\rm K}^{\rm He^+} - S_{\rm K}^{\rm H^+})\right] . \quad \text{(A4)}$$

In addition to the above constraint, the $\rm He^{++}$ filling factor $Q_{\rm He^{++}}$ is limited to be less than $Q_{\rm H^+}$. Therefore, if $Q_{\rm He^{++}} = Q_{\rm H^+}$, we require $dQ_{\rm He^{++}}/dz = dQ_{\rm H^+}/dz$ so that the fronts propagate at the same rate, and $dQ_{\rm He^+}/dz = 0$ since the $\rm He^+$ front cannot propagate if the He II region is filling all of the available volume. These constraints yield

$$\Delta\frac{dn_\gamma^{\rm He^+}}{dz} = \frac{n_{\rm He}^0 F_{\rm He^+} n_{\rm H}^0 F_{\rm H^+}}{2n_{\rm He}^0 F_{\rm He^{++}} + n_{\rm H}^0 F_{\rm H^+}}\left[(S_{\rm C}^{\rm He^{++}} - S_{\rm C}^{\rm H^+}) - (S_{\rm K}^{\rm He^{++}} - S_{\rm K}^{\rm H^+})\right]$$
$$- n_{\rm He}^0 F_{\rm He^+}\frac{n_{\rm He}^0 F_{\rm He^{++}} + n_{\rm H}^0 F_{\rm H^+}}{2n_{\rm He}^0 F_{\rm He^{++}} + n_{\rm H}^0 F_{\rm H^+}}\left[(S_{\rm C}^{\rm He^{++}} - S_{\rm C}^{\rm He^+}) - (S_{\rm K}^{\rm He^{++}} - S_{\rm K}^{\rm He^+})\right] ,$$
$$\Delta\frac{dn_\gamma^{\rm He^{++}}}{dz} = n_{\rm He}^0 F_{\rm He^{++}}\left[(S_{\rm C}^{\rm He^{++}} - S_{\rm C}^{\rm He^+}) - (S_{\rm K}^{\rm He^{++}} - S_{\rm K}^{\rm He^+}) + \frac{1}{n_{\rm He}^0 F_{\rm He^+}}\Delta\frac{dn_\gamma^{\rm He^+}}{dz}\right] . \quad \text{(A5)}$$

A2. CASE II: POST HYDROGEN OVERLAP: IF $Q_{\rm H^+} = 1$ AND $F_{\rm H^+} > F_M(\Delta_{\rm crit})$ AND [$Q_{\rm He^{++}} < 1$ OR $F_{\rm He^{++}} < F_M(\Delta_{\rm crit})$]

Following the overlap of H II regions, the mass fraction of hydrogen $F_{\rm H^+}$ is free to evolve according to equation (7) (with modified source term to account for the excess ionizing photons). The filling factors $Q_{\rm H^+}$, $Q_{\rm He^+}$, and $Q_{\rm He^{++}}$ again evolve according to a generalization of equation (4). Note that if $Q_i = 1$, substitution of equation (4) into equation (7) yields $dQ_i/dz = 0$. Thus, post H II overlap the value of $Q_{\rm H^+}$ remains at unity. However by continuing to follow all the equations we allow for the possibility of a recombination epoch following an early reionization. We have

$$\frac{dF_{\rm H^+}}{dz} = S_{\rm CF}^{\rm H^+} + \frac{1}{n_{\rm H}^0}\Delta\frac{dn_\gamma^{\rm He^+}}{dz} - S_{\rm KF}^{\rm H^+} ,$$
$$\frac{dF_{\rm He^+}}{dz} = \frac{d}{dz}F_M(\Delta_{\rm crit})F_{\rm He^+} = F_M(\Delta_{\rm crit}) ,$$
$$\frac{dF_{\rm He^{++}}}{dz} = \frac{d}{dz}F_M(\Delta_{\rm crit})F_{\rm He^{++}} = F_M(\Delta_{\rm crit}) ,$$
$$\frac{dQ_{\rm H^+}}{dz} = S_{\rm C}^{\rm H^+} + \frac{1}{n_{\rm H}^0 F_{\rm H^+}}\Delta\frac{dn_\gamma^{\rm He^+}}{dz} - S_{\rm K}^{\rm H^+} ,$$
$$\frac{dQ_{\rm He^+}}{dz} = S_{\rm C}^{\rm He^+} - \frac{1}{n_{\rm He}^0 F_{\rm He^+}}\Delta\frac{dn_\gamma^{\rm He^+}}{dz} - S_{\rm K}^{\rm He^+} - \frac{dQ_{\rm He^{++}}}{dz} ,$$
$$\frac{dQ_{\rm He^{++}}}{dz} = S_{\rm C}^{\rm He^{++}} - S_{\rm K}^{\rm He^{++}} . \quad \text{(A6)}$$

As before, the values of the excess ionizing photon rates are determined from constraints on the coevolution of the ionization fronts. In the case where $Q_{\mathrm{He}^{++}} < Q_{\mathrm{H}^+}$, Q_{He^+} is limited to be smaller than $Q_{\mathrm{He}^+} = Q_{\mathrm{H}^+} - Q_{\mathrm{He}^{++}}$. However as mentioned above, if $Q_{\mathrm{H}^+} = 1$, then the above equations imply $dQ_{\mathrm{H}^+}/dz = 0$. We therefore have $dQ_{\mathrm{He}^+}/dz = -dQ_{\mathrm{He}^{++}}/dz$, and since $\Delta\left(dn_\gamma^{\mathrm{He}^{++}}/dz\right) = 0$ in this case, we find

$$\Delta\frac{dn_\gamma^{\mathrm{He}^+}}{dz} = n_{\mathrm{He}}^0 F_{\mathrm{He}^+}\left(S_{\mathrm{C}}^{\mathrm{He}^+} - S_{\mathrm{K}}^{\mathrm{He}^+}\right) . \tag{A7}$$

A3. CASE 3: POST HELIUM OVERLAP: IF $Q_{\mathrm{He}^{++}} = 1$ AND $F_{\mathrm{He}^{++}} \geq F_M(\Delta_{\mathrm{crit}})$

Finally, following the overlap of He II regions, the mass fractions F_{H^+}, F_{He^+}, and $F_{\mathrm{He}^{++}}$ are free to evolve according to equation (7) (with modified source terms to account for the excess ionizing photons). The filling factors Q_{H^+}, Q_{He^+}, and $Q_{\mathrm{He}^{++}}$ still evolve according to generalizations of equation (4). At the point of He^{++} overlap, our formalism demands that there is no He^+ in the universe since $Q_{\mathrm{He}^+} = 0$. However, following He^{++} overlap the He^+ front (which must lead the He^{++} front) is free to propagate into the denser IGM. Therefore, following the overlap of He^{++}, F_{He^+} becomes the fraction of helium in the universe (equal to zero initially) that is singly ionized. The recombination rate R^{He^+} is calculated

$$R^{\mathrm{He}^+} = \int_{\Delta_i^{\mathrm{He}^{++}}}^{\Delta_i^{\mathrm{He}^+}} d\Delta\frac{dP}{d\Delta}\Delta^2 , \tag{A8}$$

where $F_{\mathrm{He}^{++}} = \int_0^{\Delta_i^{\mathrm{He}^{++}}} d\Delta(dP/d\Delta)\Delta$ and $F_{\mathrm{He}^{++}} + F_{\mathrm{He}^+} = \int_0^{\Delta_i^{\mathrm{He}^+}} d\Delta(dP/d\Delta)\Delta$. As before, if $Q_i = 1$ substitution of equation (4) into equation (7) yields $dQ_i/dz = 0$. The filling factors Q_{H^+} and $Q_{\mathrm{He}^{++}}$ therefore remain at unity. We have

$$\begin{aligned}
\frac{dF_{\mathrm{H}^+}}{dz} &= S_{\mathrm{CF}}^{\mathrm{H}^+} + \frac{1}{n_{\mathrm{H}}^0}\left(\Delta\frac{dn_\gamma^{\mathrm{He}^+}}{dz} + \Delta\frac{dn_\gamma^{\mathrm{He}^{++}}}{dz}\right) - S_{\mathrm{KF}}^{\mathrm{H}^+} ,\\
\frac{dF_{\mathrm{He}^+}}{dz} &= S_{\mathrm{CF}}^{\mathrm{He}^+} - \frac{1}{n_{\mathrm{He}}^0}\Delta\frac{dn_\gamma^{\mathrm{He}^+}}{dz} - S_{\mathrm{KF}}^{\mathrm{He}^+} - \frac{dF_{\mathrm{He}^{++}}}{dz} ,\\
\frac{dF_{\mathrm{He}^{++}}}{dz} &= S_{\mathrm{CF}}^{\mathrm{He}^{++}} - \frac{1}{n_{\mathrm{He}}^0}\Delta\frac{dn_\gamma^{\mathrm{He}^{++}}}{dz} - S_{\mathrm{KF}}^{\mathrm{He}^{++}} ,\\
\frac{dQ_{\mathrm{H}^+}}{dz} &= S_{\mathrm{C}}^{\mathrm{H}^+} + \frac{1}{n_{\mathrm{H}}^0 F_{\mathrm{H}^+}}\left(\Delta\frac{dn_\gamma^{\mathrm{He}^+}}{dz} + \Delta\frac{dn_\gamma^{\mathrm{He}^{++}}}{dz}\right) - S_{\mathrm{K}}^{\mathrm{H}^+} ,\\
\frac{dQ_{\mathrm{He}^+}}{dz} &= S_{\mathrm{C}}^{\mathrm{He}^+} - \frac{1}{n_{\mathrm{He}}^0 F_{\mathrm{He}^+}}\Delta\frac{dn_\gamma^{\mathrm{He}^+}}{dz} - S_{\mathrm{K}}^{\mathrm{He}^+} - \frac{dQ_{\mathrm{He}^{++}}}{dz} ,\\
\frac{dQ_{\mathrm{He}^{++}}}{dz} &= S_{\mathrm{C}}^{\mathrm{He}^{++}} - \frac{1}{n_{\mathrm{He}}^0 F_{\mathrm{He}^{++}}}\Delta\frac{dn_\gamma^{\mathrm{He}^{++}}}{dz} - S_{\mathrm{K}}^{\mathrm{He}^{++}} .
\end{aligned} \tag{A9}$$

The excess ionizing photon rates are determined as follows. If $F_{\mathrm{He}^{++}} < F_{\mathrm{H}^+}$, then F_{He^+} is limited to be smaller than $F_{\mathrm{He}^+} = F_{\mathrm{H}^+} - F_{\mathrm{He}^{++}}$ since the He^+ front cannot propagate beyond the H^+ front. Therefore, if $F_{\mathrm{He}^+} = F_{\mathrm{H}^+} - F_{\mathrm{He}^{++}}$, we require $dF_{\mathrm{He}^+}/dz = dF_{\mathrm{H}^+}/dz - dF_{\mathrm{He}^{++}}/dz$, and since $\Delta\left(dn_\gamma^{\mathrm{He}^{++}}/dz\right) = 0$ in this case, we find

$$\Delta\frac{dn_\gamma^{\mathrm{He}^+}}{dz} = \left(\frac{1}{n_{\mathrm{He}}^0} + \frac{1}{n_{\mathrm{H}}^0}\right)^{-1}\left[\left(S_{\mathrm{CF}}^{\mathrm{He}^+} - S_{\mathrm{CF}}^{\mathrm{H}^+}\right) - \left(S_{\mathrm{KF}}^{\mathrm{He}^+} - S_{\mathrm{KF}}^{\mathrm{H}^+}\right)\right] . \tag{A10}$$

The He^{++} mass fraction $F_{\mathrm{He}^{++}}$ is limited to be less than F_{H^+}. Therefore, if $F_{\mathrm{He}^{++}} = F_{\mathrm{H}^+}$, we require $dF_{\mathrm{He}^{++}}/dz = dF_{\mathrm{H}^+}/dz$ so that the fronts propagate at the same rate, and $dF_{\mathrm{He}^+}/dz = 0$ since the He^+ front cannot grow if the He^{++} is filling all of the available volume. These constraints yield

$$\begin{aligned}
\Delta\frac{dn_\gamma^{\mathrm{He}^+}}{dz} = {} & \frac{n_{\mathrm{He}}^0 n_{\mathrm{H}}^0}{2n_{\mathrm{He}}^0 + n_{\mathrm{H}}^0}\left[\left(S_{\mathrm{CF}}^{\mathrm{He}^{++}} - S_{\mathrm{CF}}^{\mathrm{H}^+}\right) - \left(S_{\mathrm{KF}}^{\mathrm{He}^{++}} - S_{\mathrm{KF}}^{\mathrm{H}^+}\right)\right]\\
& - n_{\mathrm{He}}^0\frac{n_{\mathrm{He}}^0 + n_{\mathrm{H}}^0}{2n_{\mathrm{He}}^0 + n_{\mathrm{H}}^0}\left[\left(S_{\mathrm{CF}}^{\mathrm{He}^{++}} - S_{\mathrm{CF}}^{\mathrm{He}^+}\right) - \left(S_{\mathrm{KF}}^{\mathrm{He}^{++}} - S_{\mathrm{KF}}^{\mathrm{He}^+}\right)\right] ,\\
\Delta\frac{dn_\gamma^{\mathrm{He}^{++}}}{dz} = {} & n_{\mathrm{He}}^0\left[\left(S_{\mathrm{CF}}^{\mathrm{He}^{++}} - S_{\mathrm{CF}}^{\mathrm{He}^+}\right) - \left(S_{\mathrm{KF}}^{\mathrm{He}^{++}} - S_{\mathrm{KF}}^{\mathrm{He}^+}\right) + \frac{1}{n_{\mathrm{He}}^0}\Delta\frac{dn_\gamma^{\mathrm{He}^+}}{dz}\right] .
\end{aligned} \tag{A11}$$

REFERENCES

Abel, T., Bryan, G. L., & Norman, M. L. 2000, ApJ, 540, 39
Bardeen, J. M., Bond, J. R., Kaiser, N., & Szalay, A. S. 1986, ApJ, 304, 15
Barkana, R., & Loeb, A. 2001, Phys. Rep., 349, 125
Becker, R. H., et al. 2001, AJ, 122, 2850
Bell, E. F., & de Jong, R. S. 2001, ApJ, 550, 212
Bond, J. R., et al. 2002, ApJ, submitted (astro-ph/0205386)
Boyle, B. J., Shanks, T., Croom, S. M., Smith, R. J., Miller, L., Loaring, N., & Heymans, C. 2000, MNRAS, 317, 1014
Bromm, V., Coppi, P. S., & Larson, R. B. 1999, ApJ, 527, L5
———. 2001, preprint (astro-ph/0102503)
Bromm, V., Ferrara, A., Coppi, P. S., & Larson, R. B. 2001, MNRAS, 328, 969
Bromm, V., Kudritzki, R. P., & Loeb, A. 2001, ApJ, 552, 464
Davidsen, A. F., Kriss, G. A., & Zheng, W. 1996, Nature, 380, 47
Dekel, A., & Silk, J. 1986, ApJ, 303, 39
Fan, X., Narayanan, V. K., Strauss, M. A., White, R. L., Becker, R. H., Pentericci, L., & Rix, H. 2002, AJ, 123, 1247
Fan, X., et al. 2001a, AJ, 121, 54
———. 2001b, AJ, 122, 2833
Ferrarese, L. 2002, preprint (astro-ph/0203469)
Gruzinov, A., & Hu, W. 1998, ApJ, 508, 435
Gunn, J. E., & Peterson, B. A. 1965, ApJ, 142, 1633
Haiman, Z., & Loeb, A. 1997, ApJ, 483, 21
Heap, S. R., Williger, G. M., Smette, A., Hubeny, I., Sahu, M. S., Jenkins, E. B., Tripp, T. M., & Winkler, J. N. 2000, ApJ, 534, 69
Hogan, C. J., Anderson, S. F., & Rugers, M. H. 1997, AJ, 113, 1495
Hu, W. 2000, ApJ, 529, 12
Hu, W., & White, M. 1997, ApJ, 479, 568
Jacobsen, P., et al. 1994, Nature, 370, 35
Kamionkowski, M., Kosowsky, A., & Stebbins, A. 1997, Phys. Rev. D, 55, 7368
Kaplinghat, M., Chu, M., Haiman, Z., Holder, G., Knox, L., & Skordis, C. 2002, preprint (astro-ph/0207591)
Kauffmann, G., et al. 2003, MNRAS, in press
Kriss, G. A., et al. 2001, Science, 293, 1112
Leitherer, C., et al. 1999, ApJS, 123, 3
Mackey, J., Bromm, V., Hernquist, L. 2002, preprint (astro-ph/0208447)
Madau, P., Haardt, F., & Rees, M. J. 1999, ApJ, 514, 648
Miralda-Escudé, J., Haehnelt, M., & Rees, M. J. 2000, ApJ, 530, 1
Oh, S. P., Nollett, K. M., Madau, P., & Wasserburg, G. J. 2001, ApJ, 562, L1
Osterbrock, D. E. 1974, Astrophysics of Gaseous Nebulae (San Francisco: Freeman), chap. 2
Padin, S., et al. 2001, ApJ, 549, L1
Press, W. H., & Schechter, P. 1974, ApJ, 187, 425
Reimers, D., et al. 1997, A&A, 327, 890
Scalo, J. 1998, in ASP Conf. Ser. 142, The Stellar Initial Mass Function: 38th Herstmonceux Conference, ed. G. Gilmore & D. Howell (San Francisco: ASP), 201
Scannapieco, E., Ferrara, A., & Madau, P. 2002, ApJ, 574, 590
Schaye, J., Theuns, T., Rauch, M., Efstathiou, G., & Sargent, W. L. W. 2000, MNRAS, 318, 817
Schirber, M., & Bullock, J. S. 2002, preprint (astro-ph/0207200)
Sheth, R. K., & Tormen, G. 1999, MNRAS, 308, 119
Smette, A., Heap, S. R., Williger, G. M., Tripp, T. M., Jenkins, E. B., & Songaila, A. 2002, ApJ, 564, 542
Songaila, A. 2001, ApJ, 561, L153 (erratum 568, L139)
Steidel, C., et al. 2002, preprint (astro-ph/0205142)
Theuns, T., Bernardi, M., Frieman, J., Hewett, P., Schaye, J., Sheth, R. K., & Subbarao, M. 2002, ApJ, 574, L111
Thoul, A. A., & Weinberg, D. H. 1996, ApJ, 465, 608
Tytler, D. 1995, in QSO Absorption Lines, Proc. ESO Workshop, ed. G. Meylan (Berlin: Springer), 289
Wang, X., Tegmark, M., & Zaldarriaga, M. 2002, Phys. Rev. D, 65, 123001
Wood, K., & Loeb, A. 2000, ApJ, 545, 86
Wyithe, J. S. B., & Loeb, A. 2002, preprint (astro-ph/0206154)
Zaldarriaga, M., & Seljak, U. 1997, Phys. Rev. D, 55, 1830

REFERENCES:
1. Commentary on the Jeans (1902) theory of gravitational structure formation. Journal of Cosmology (2011), Vol. 17, No. 15, pp 7430-7484. The link is http://JournalofCosmology.com/JoC17pdfs GibComJeans 1902_90845.pdf.
2. Commentary on the Gibson (1996) fluid mechanical theory of cosmic structure formation. Journal of Cosmology (2011), Vol. 17, No. 16, pp 7485-7523.
3. Commentary on Schild (1996) first detection and identification of earth-mass dark matter planets as the missing mass of a galaxy lensing a quasar. Journal of Cosmology (2011), Vol. 17, No. 17, pp 7424-7530.